Tellus (2008), 60A, 459–491
Printed in Singapore. All rights reserved

TELLUS

Aerosol-climate interactions in the CAM-Oslo atmospheric GCM and investigation of associated basic shortcomings

By ØYVIND SELAND*, TROND IVERSEN[1], ALF KIRKEVÅG and TRUDE STORELVMO[1,2],
Norwegian Meteorological Institute, P.O. Box 43 Blindern, 0313 Oslo, Norway

(Manuscript received 3 May 2007; in final form 7 January 2007)

ABSTRACT

The paper discusses some challenges in aerosol-climate modelling. CAM-Oslo, extended from NCAR-CAM3, employs an aerosol module for sea-salt, dust, sulphate, black carbon (BC) and particulate organic matter (OM). Primary aerosol size-distributions are modified by condensation, coagulation and wet-phase processes. Aerosol optics and cloud droplet numbers use look-up tables constructed from first principles. Ground level sulphate and sea-salt are generally well modelled, BC and OM are slightly underestimated (uncertain), and dust is considerably (factor ∼2) underestimated. Since non-desert dust, nitrate, anthropogenic secondary organics, and biological particles are omitted, aerosol optical depths (0.12) are underestimated by 10–25%. The underestimates are large in areas with biomass burning and soil dust. The direct and indirect forcing of aerosol increments since pre-industrial time are estimated at $+0.031\,\mathrm{Wm}^{-2}$ and $-1.78\,\mathrm{Wm}^{-2}$, respectively. Although the total absorption AOD probably is slightly underestimated, the BC contributes to DRF with double strength compared to the AeroCom average. Main reasons for this include: internal BC-mixing ($+0.2\,\mathrm{Wm}^{-2}$), accumulation mode BC-agglomerates ($+0.05\,\mathrm{Wm}^{-2}$), assumed aitken-mode OM-BC mixture ($+0.1\,\mathrm{Wm}^{-2}$), large BC fraction (36%) above 500 hPa, and high low-level cloudiness. Using a prognostic CDNC and process parametrized CCN activation instead of assuming CDNC are equal to CCN, the indirect forcing is 36% smaller.

1. Introduction

Aerosol particles and their interactions with clouds and radiation constitute a major source of uncertainty in the understanding of basic mechanisms and the modelling of natural and anthropogenic climate forcings. This has been carefully demonstrated in the recent and still ongoing AeroCom inter-comparison exercise (Kinne et al., 2006; Textor et al., 2006 & 2007; Schulz et al., 2006; Penner et al., 2006), which also includes atmospheric global models with more advanced aerosol and atmospheric chemistry treatments than are presently used in coupled climate models for transient climate projections.

The same mass concentration of a particulate constituent can interact in a wide range of ways with solar radiation or produce vastly different numbers of cloud condensation nuclei (CCN). Size distributed aerosol number concentrations and particle compositions are potentially more important than the mass concentration itself (e.g. Dusek et al., 2006). Also the vertical distribution profile for absorbing aerosols, such as black carbon (BC), can strongly influence the forcing of the same total column of aerosol particle mass, and even quantities not related to aerosols at all can change the aerosol forcing considerably, such as the ground-surface albedo (e.g. Iversen et al., 2005).

Aerosol particles have a huge variety in size and mixing state between various chemical compounds, including water. The ability of a particle to influence electromagnetic radiation varies strongly with its size and composition. In particular, the relative amount of scattering vs. absorptive materials in an internal mixture is important, as emphasized in a number of earlier studies (e.g. Cooke and Wilson, 1996; Iversen et al., 2001; Jacobson, 2001). Furthermore, activation of a particle as a CCN which contributes to the CDNCs depends on its size and hygroscopic property. Although not included in this study, activation of aerosols as ice nuclei depends on the crystal structure of the solid material in the particles. This multifaceted importance of the physical properties of aerosols, ideally calls for a fine resolution sectional description of aerosol size distributions with respect to number and composition. With current computer

*Corresponding author.
e-mail: oyvind.seland@met.no
[1]Original address: Department of Geosciences, University of Oslo, P.O. Box 1022 Blindern, 0315 Oslo, Norway.
[2]Present address: Institute for Atmospheric and Climate Science, ETH-Zurich, Zürich, Switzerland
DOI: 10.1111/j.1600-0870.2008.00318.x

resources, however, such detail is not practically possible in climate models.

In this paper we study how some assumptions related to aerosol particle size and vertical distribution, as well as cloud droplets developments, can influence the model calculations of aerosol–climate interactions in a global atmospheric climate model. To meet the need for detailed descriptions of aerosols in an approximate way, we employ a further elaborated version of the aerosol module described in Iversen and Seland (2002 and 2003), Kirkevåg and Iversen (2002), and Kristjánsson (2002). The model is a version of the Community Atmospheric Model 3 (CAM3) of the National Center for Atmospheric Research (NCAR) extended with our own developed module for aerosol life-cycles and interactions with radiation and clouds. We denote this model version CAM-Oslo. CAM-Oslo and the aerosol module in particular, uses concepts and methods of the earlier version CCM-Oslo based on NCAR CCM3. CCM-Oslo included particulate sulphate and BC (Iversen and Seland, 2002 and 2003, Kirkevåg and Iversen, 2002; Kristjánsson, 2002) and was later extended with particulate organic matter (OM) (Kirkevåg et al., 2005), and it was coupled to a slab ocean for equilibrium climate simulations (Kristjánsson et al., 2005; Kirkevåg et al., 2008a). Using CCM-Oslo we have contributed to the AeroCom intercomparison (Kinne et al., 2006; Textor et al., 2006; Schulz et al., 2006). An intermediate version of CAM-Oslo was based on NCAR CAM2 and included prognostic equations for CDNCs together with the same aerosol scheme as in CCM-Oslo (Storelvmo et al., 2006; Penner et al., 2006). Due to the more complex structure of the aerosol parameterization in CAM-Oslo compared to CCM-Oslo, only a preliminary version of the prognostic equation for cloud droplet number is available at present time. Results from a simulation with the updated parameterization are presented in a sensitivity test.

The present version of CAM-Oslo performs prognostic calculations of the natural primary aerosols sea-salt (SS) and mineral dust (DU), includes a sulphur cycle with gaseous precursors (DMS and SO_2) yielding sulphate (SO_4), and calculates BC and particulate OM. So far the model uses the standard cloud microphysics scheme (Rasch and Kristjánsson, 1998) in conjunction with a CDNC parameterization based on the CCM-Oslo scheme (Kristjánsson, 2002; Kirkevåg et al., 2005). Oxidants in the sulphur scheme are prescribed (Berntsen and Isaksen, 1997). Although the principles have been developed independently, the aerosol module has many similarities with that of Stier et al. (2005). The chemical components and the size modes are the same in the two models, but CAM-Oslo does not solve equations for number concentrations. A 44 bin sectional model is used to construct look-up tables for aerosol optical properties and activated CCN (Kirkevåg et al., 2005). Hence, both the direct climate effects as well as the first (Twomey, 1977) and second (Albrecht, 1989) indirect effects can be estimated. As listed in Textor et al. (2007), most models which address the aerosol–climate interactions globally prescribe size-distributions and particle mixing state. The GISS ModelE, for example, assumes externally mixed aerosols, and does not calculate aerosol size except for SS (Koch et al., 2006; Schmidt et al., 2006). The CAM-Oslo presented in this paper and the recent ECHAM HAM (Stier et al., 2005) both produce size distributed number concentrations and particle composition from basic physico-chemical processes, although the approaches are different.

The number of retrievals of remote sensing instruments designed for characterizing aerosol properties has increased considerably during the last 5 yr (Liu et al., 2006). These include satellites (http://modis.gsfc.nasa.gov, http://www-misr.jpl.nasa.gov) and ground based sun photometers (http://aeronet.gsfc.nasa.gov) and lidars (http://www.earlinet.org). Nevertheless, there is a considerable lack of in situ observations of size-segregated number and mass concentrations, in particular in the free troposphere. Careful field and laboratory studies for the purpose of constraining the range of process-specific uncertainties in the models are also too few (see Dusek et al. (2006) as an example). As emphasized by, for example Lohmann and Feichter (2005), uncertain processes in models should be constrained to suitably detailed observations or laboratory studies, whilst retrievals of bulk quantities should only be used for comparison with similar model-generated quantities.

The retrievals of bulk properties leave a risk that corresponding model-calculated bulk properties can be considered to be approximately correct in cases where there are huge but compensating errors. Adjustment of uncertain parameters ('tuning') to obtain good comparison with retrievals of bulk properties will probably lead to such errors. The main concern is that errors and shortcomings in models can be hidden as a consequence of the validation procedure rather than receiving increased attention. Although this has a much wider relevance than aerosol–climate interactions, results from AeroCom indicate that this is a reality in models addressing this issue. The relative spread between models is not larger for quantities calculated towards the end of the process-chain (e.g. direct forcing) than for first order quantities (emissions and concentrations) (Textor et al., 2006, 2007; Schulz et al., 2006). In this work, we try to follow the principles stated by Lohmann and Feichter (2005) in the modelling and validation of the aerosols, in order to more explicitly focus on areas which need further research attention. We admit that this principle is difficult to follow even to some extent, since any model aimed at realistic simulations of wide aspects of the climate will have to choose values for many uncertain parametric representations. However, the impacts of such uncertainties should be investigated by a probabilistic approach to climate predictions as done in the last report of IPCC (Solomon et al., 2007). One possible sign of compensating errors in aerosol–climate modelling is that many models produce reasonably correct aerosol optical depths (AOD) compared to retrievals from satellites or from Aeronet, despite that some aerosol components are commonly neglected. At present, most models neither include particulate nitrate nor particles of biologic origins (Jaenicke, 2005), and

emissions of soil dust of non-desert origins are probably underestimated in, for example the AeroCom emissions of Dentener et al. (2006).

The calculations of aerosol effects in this paper are done off-line, that is aerosol effects on radiation and parameterization of cloud-microphysics do not influence to the driving meteorology of the model. Simulations are also made in climate modus, that is there is no assimilation of observed data or nudging to analyses. The use of fixed sea-surface temperatures of the present day nevertheless controls the climate development to a considerable degree. An on-line version of the climate-aerosol model coupled to a slab ocean model is presented in the accompanying paper of Kirkevåg et al. (2008b).

2. Model description

2.1. The CAM3 general circulation model

The atmospheric general circulation model is based on the sixth generation of the Community Atmospheric Model, NCAR-CAM3 (Collins et al., 2006a, b). CAM3 can be run either as a stand-alone AGCM, or as a component of the Community Climate System Model coupled to other compartments of the climate system. It can also be run with a slab ocean model for equilibrium climate response studies (Kirkevåg et al., 2008b). As stand-alone model CAM3 is integrated with the Community Land Model, a thermodynamic sea ice model, and a data ocean. The version used in this work uses the Eulerian dynamical core at T42 spectral truncation, which is approximately $2.8 \times 2.8^{\circ}$ on a Gaussian grid. The model uses a hybrid η-coordinate with 26 levels in the vertical. An important change from CCM3 (Kiehl et al., 1998) to CAM3 is that the diagnostic cloud water scheme is replaced by the prognostic cloud-water parameterization of Rasch and Kristjánsson (1998) updated by Zhang et al. (2003). CAM3 also includes separate evolution equations for the liquid and ice-phase condensate. CAM3 has generally both a much higher total cloud-fraction and LWP than CCM3 (Boville et al., 2006). The increased cloud-fraction leads to more efficient aqueous-phase oxidation and aerosol coagulations with cloud droplets, as well as affecting the wet scavenging of soluble contaminants. The parameterization of deep convection in CAM3 is similar to CCM3 (Zhang and McFarlane, 1995), but with the addition that the convective cloud fraction is explicitly included in CAM3.

In the CAM-Oslo version of CAM3, we have introduced a module for aerosol life-cycling and interactions with radiation and clouds; see Sections 2.4–2.8. In addition, the parameterization of clouds and precipitation are slightly modified, as described in sections 2.2 and 2.3 below.

2.2. Changes in auto-conversion

When the original cloud module in CAM3 was used in simulations with aerosols run on-line with meteorology in CAM-Oslo, Kirkevåg et al. (2008b) found that the CDNCs yielded reduced liquid water path (LWP) in temperate and polar climates compared to off-line simulations. The reason for this is that the standard predefined aerosol, which is used to calculate precipitation rate and to influence the radiative budget in CAM3, produce more numerous cloud droplets than the CAM-Oslo aerosol life-cycle does on average. Hence, when our aerosol module is run on-line, cloud droplets are fewer and larger, and auto-conversion is increased if no other parameters are adjusted. To reduce this difference in LWP between the original CAM3 and the on-line version of CAM-Oslo, Kirkevåg et al. (2008b) adjusted the auto-conversion formulation. For reasons of consistency, the same parameterization is used in this work.

The auto-conversion of cloud droplets to precipitation in warm clouds is the only possible source of a second indirect aerosol effect in the present version of CAM-Oslo. Based on original proposals by Chen and Cotton (1987) the scheme was formulated for the NCAR community climate model by Rasch and Kristjánsson (1998). Important parameters in the scheme are the cloud liquid water content, the CDNCs, the factor $C_{l,aut}$ proportional to the collection efficiency of falling precipitation through a population of cloud droplets, and the critical mean volume radius of cloud droplets ($r_{\forall c}$) for onset of auto-conversion (Rasch and Kristjánsson, 1998). Applying prescribed CDNCs, Rasch and Kristjánsson (1998) used $r_{\forall c} = 5\ \mu$m, and a factor 10 reduction of $C_{l,aut}$ if the entering precipitation rate was smaller than $P_{aut,c} = 0.5$ mm day^{-1}. The latter quantity, the critical precipitation rate for enhanced auto-conversion$P_{aut,c}$, is tuned to reduce precipitation rates and thus avoid too small droplets (Baker, 1993). In the original CAM3 from NCAR (Collins et al., 2004), $r_{\forall c} = 10\ \mu$m and $P_{aut,c} = 0.5$ mm day^{-1}. With CDNC calculated from an on-line aerosol module Kristjánsson (2002) and Kristjánsson et al. (2005) used $r_{\forall c} = 10\ \mu$m and $P_{aut,c} = 5.0$ mm day^{-1} with reasonable results for the droplet size and precipitation rate.

In this work, we follow the recommendation by Collins et al. (2004) and use $r_{\forall c} = 15\ \mu$m and $P_{aut,c} = 5.0$ mm day^{-1}, which yields a ca. 30% increased globally averaged cloud LWP compared to the original CAM3 (Collins et al., 2004). As shown in Section 4 below, an increased LWP reduces the scavenging efficiency of particles and the second indirect effect. It should be noted that $P_{aut,c}$ probably will be reduced as the aerosol scheme in CAM-Oslo becomes more complete and will include nitrate and other hygroscopic aerosol compounds.

2.3. "Freeze-dry" parameterization of polar clouds

In the winter-time Arctic boundary layer, however, cloudiness is considerably overestimated in CAM3, as it also was in CCM3. This can potentially be associated with underestimated contaminant levels in the Arctic boundary layer in winter and spring in the earlier CCM-Oslo (Iversen and Seland, 2002 & 2003). We have included an adjustment of the parameterization of

fractional cloudiness as suggested by S. Vavrus (personal communication), as described in section 2.3 below. Partly inspired by Xu and Randall (1996) the low-level cloudiness is adjusted (below model level $\eta = 0.75$) for very low absolute water vapour content. The reduced boundary layer cloudiness is an attempt to include the direct scavenging of water vapour in very cold air, that is dehydration or 'freeze-dry'. For water vapour mass mixing ratios lower than $q_c = 3$ g/kg air, the low-level cloud cover is reduced to $cl_{vap} = cl_{orig} * q/q_c$. The cloud cover is never reduced more than 85% compared to the original.

2.4. Aerosol emissions and life-cycle

Seven types of components are calculated in the aerosol life-cycle scheme. SS (SS) and mineral soil dust (DU), BC, particulate OM, particulate sulphate (SO_4) and the gaseous precursors di-methyl-sulphide (DMS) and sulphur dioxide (SO_2). Potentially important aerosols which, at present, are not included are particulate nitrate, biological particles and certain types of non-desert soil dust.

A schematic of the aerosol module including all the calculated components, the chemical production, and the physical processes causing transfer between the components, is given in Fig. 1. Major extensions compared to Iversen and Seland (2002 and 2003) include new prognostic compounds in the life-cycling (SS, DU, OM), the introduction of the aitken mode, and a wide range of internally mixed particle types. The module calculates the mass concentrations of a number of aerosol components. These concentrations are categorized, or tagged, according to the size mode (nucleation, aitken, accumulation, coarse) and production mechanism (nucleation, condensation, coagulation, aqueous chemistry) of the particle mass. The tagged information is transported along with the species. Hence, as illustrated in Fig. 1, a considerable number of variables are dedicated to each of the basic aerosol components SS, DU, SO_4, BC and OM. Assumed size-distributions of primary emitted or nucleated particles are basic in the determination of particle number concentrations. These primary particles are three modes of SS, two modes of DU, two modes of SO_4, two modes of BC, one mode of OM and one mode of emitted internally mixed OM and BC. Total number of transported species is 26. Table 1 shows assumed initial size-distributions for the primary and nucleated particles. As seen from Table 2, all compounds except DMS are subject to both dry deposition and wet scavenging.

The starting point of the aerosol life-cycle module is the emissions taken from Dentener et al. (2006) and used in the AeroCom project. They included estimates present-day (2000) and pre-industrial (1750) aerosol and aerosol precursor emissions, enabling calculation of industrial anthropogenic aerosol burdens, and the impacts of these anthropogenic aerosols on climate. Modal parameters for the log-normal modes used to characterize emissions, are given in Table 1, but it is emphasized that

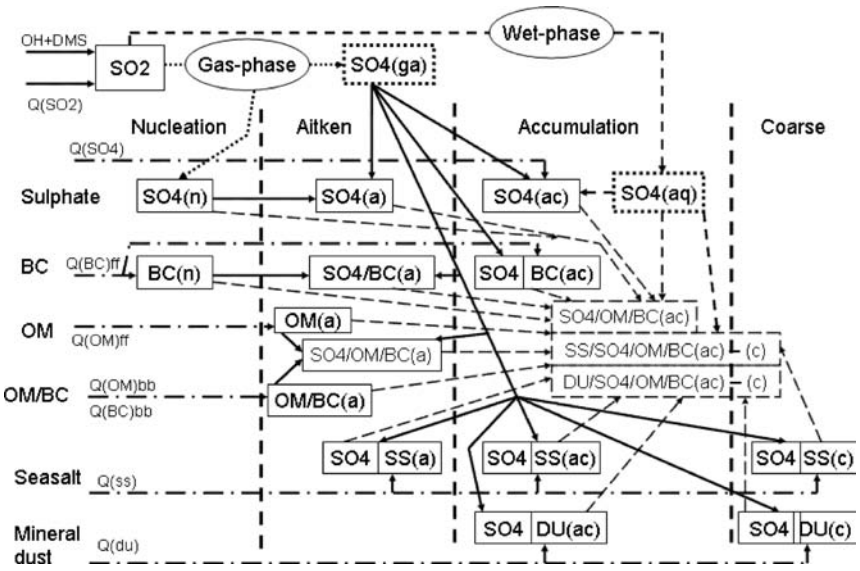

Fig. 1. Schematic for aerosol particle processing in CAM-Oslo. Primary particles are emitted (dashed-dotted arrows) as accumulation-mode sulphate (SO_4(ac)), nucleation and accumulation mode black carbon (BC(n), BC(ac)), aitken mode organic matter, (OM(a)), internally mixed aitken mode OM and BC (OM/BC(a)), aitken, accumulation, and coarse mode sea-salt (SS(a), SS(ac), SS(c)), accumulation and coarse mode mineral dust (DU(ac), DU(c)). Model calculated gas-phase components are DMS and SO_2. Gaseous sulphate (SO_4(ga)) produced in clear air is immediately transformed to nucleation-mode sulphate (SO_4(n), dotted arrow) in cases when there is insufficient pre-existing particle surface area available for condensation (continuous arrows). Sulphate produced by oxidation in cloud droplets (SO_4(aq), short-dashed arrow) is partly added to SO_4(ac) but mainly to a broad internal mixture of accumulation and coarse mode particles (compounds in dashed rectangles of which there are three types). Long-dashed arrows represent coagulation processes also contributing to the latter particle types.

Table 1. Initial modal size parameters, mass densities and accommodation coefficients for primary emitted log-normal aerosol size modes. The aerosol compounds are explained in Fig. 1. BC(ac) is an externally mixed fractal agglomerate, hence the low density of 507 kg m^{-3}

Mode	Radius (μm)	Standard deviation	Mass density (kg m^{-3})	Accommodation coefficient for SO_4 condensation
SO4(n)	0.0118	1.8	1841	1
BC(n)			2000	0.3
OM(a)	0.04	1.8	1500	0.7
OM(a)/BC(a)			1500/2000	0.5
SO4(ac)	0.075	1.59	1769	1
BC (ac)	0.1	1.60	507	0.3
SS(a)	0.022	1.59	2200	1
SS (ac)	0.13		2200	1
DU(ac)	0.22		2600	0.3
SS(c)	0.74	2.0	2200	1
DU(c)	0.63		2600	0.3

Table 2. In-cloud scavenging coefficients and below-cloud collection efficiencies for removal by stratiform and convective precipitation. The aerosol compounds are explained in Fig. 1

Mode	In-cloud scavenging coefficient	Below-cloud collection efficiency	
		Stratiform	Convective
SO4(n)	0	0.04	0.004
BC(n)		0.08	0.008
OM(a)			
OM(a)/BC(a)	0.1	0.02	0.002
SO_4(a)			
SO_4/BC(a)	0.25	0.02	0.002
SO4/OM/BC(a)			
BC(ac)	0		
SO4/OM/BC (ac)	0.8	0.01	0.001
SS(a)			
SS/OM/BC/SO4(ac)	1	0.02	0.002
DU/OM/BC/SO4(ac)			
SS/OM/BC/SO4(c)	1	0.5	0.5
DU/OM/BC/SO4(c)	1	0.2	0.2
SO4(ga)	0.25	0.02	0.002
SO4(aq)	1	0.01	0.001

these modes are not kept during aerosol processing. Major components in the pre-industrial emissions are SS, DU, secondary organic aerosols (SOA) from biogenic processes in vegetation, natural sources and some from biomass burning (see left columns in Table 3).

All the seven basic components in the aerosol life-cycle scheme are emitted from ground-based sources, but are distributed vertically following the recommendations by Dentener et al. (2006). Some components are in addition produced chemically in the air (SO_2 and SO_4). DMS is a gas emitted from natural biogenic production in the ocean mixing layer and is depleted by oxidation to particulate MSA, which is assumed swiftly deposited, and to SO_2. Apart from being produced from DMS, SO_2 is emitted from combustion of fossil fuel and biomass containing sulphur. It has also important natural emissions from volcanoes.

A minor fraction of the sulphur emissions are sulphate produced catalytically during or immediately after combustion. This primary particulate sulphate is emitted in the accumulation mode with a modal radius of 75 nm, based on Stier et al. (2005). This is a change since Iversen and Seland (2002 and 2003) where all sulphate was assumed emitted as sulphuric acid gas.

Emissions of BC and OM from fossil fuel combustion are assumed externally mixed. Observations (Ogren and Charlson, 1983) indicate that fossil fuel BC is separated from fossil fuel OM both in its initial state and after condensation of a sulphate coating. Furthermore, whilst the main mass fraction of fossil fuel BC is assumed emitted in the nucleation mode, 10% is assumed emitted as agglomerated BC in the accumulation mode, with fractal shapes following Ström et al. (1992) with a fractal dimension of 2.5. This is consistent with a somewhat aged, but not entirely collapsed agglomerate structure. The relevance of such mode is supported by Bond and Bergstrom (2006) and Bond et al. (2006). The emitted OM from fossil fuel combustion is ca. 5% of the total OM emissions. The corresponding fraction for fossil fuel BC is almost 40%.

When emitted from biomass burning OM and BC are assumed internally mixed with each other, as recommended in Dentener et al. (2006). Externally mixed BC is assumed fully hydrophobic whilst OM is assumed to be 25% as hygroscopic as ammonium sulphate (e.g. Ghan et al., 2001). Both BC and OM turns gradually into fully hydrophilic, internally mixed aerosols when gaseous sulphate condenses on them, or by coagulation

Table 3. Calculated global annual mass budget numbers, aerosol optical depths, and mass extinction coefficients (MEC) for the individual modelled species. Simulation period: year 3–5. The upper values in a table cell are for present-day emissions and the lower for pre-industrial emissions. For gaseous precursors, the fractions of chemical loss are also included. Numbers in parenthesis give the percentage of this loss, which respectively concerns gaseous oxidation of DMS to MSA, and aqueous-phase oxidation of SO_2 to sulphate. Sources and burdens of sulphur species are given as Tg S. The SOA budget is a part of OM as indicated by the $+-$ sign. The high MEC for sea-salt is due to our slightly increased fraction of the emissions in accumulation mode. Using standard AeroCom assumptions, MEC of SS is reduced to 3.7 m^2g^{-1}

	Emissions [$Tgyr^{-1}$]								
Spec.	Total	Bio. Burn.[1] Biogenic[2] Volcanic[3]	Total Sources [Tg/yr]	Total Burden [Tg]	Life-time [days]	Wet dep. [%]	Chemical Loss [%]	Optical depth at 550 nm	MEC [m^2g^{-1}]
DMS	18.2	18.2[2]	18.1	0.10	2.09		100 (25.3)	n.a.	n.a.
SO_2	68.6	6.7[1]/14.2[3]	82.2	0.29	1.27	9.0	71.4 (85.2)	n.a.	n.a.
	14.9	0.77[1]/14.2[3]	28.4	0.084	1.08	10.0	81.0 (86.9)		
SO_4	1.8	0.17[1]/0.37[3]	60.4	0.66	3.96	92.3	n.a.	0.0253	6.51
	0.38	0.02[1]/0.37[3]	23.4	0.24	3.80	93.4		0.0079	5.51
BC	7.7	4.5[1]	7.7	0.14	6.74	75.0	n.a.	0.00195	6.94
	1.4	1.4[1]	1.4	0.027	7.08	80.8		0.00029	5.35
OM	65.6+	43.2[1]	65.6+	1.30	7.22	80.2	n.a.	0.0234	9.13
(+SOA)	33.3+	14.4[1]	33.2+	0.64	7.05	80.6		0.0091	7.26
SOA	19.1	19.1[2]	n.a.	n.a.	n.a.	n.a.	n.a.	n.a.	n.a.
SS	7925	0	7711	5.76	0.27	26.2	n.a.	0.0704	6.26
								0.0702	6.24
DU	1678	0	1671	10.40	2.27	35.9	n.a.	0.0206	1.0
								0.0198	0.96
MSA	0	0	4.6	0.021	1.67	71.7	0	n.a.	n.a.

with sulphate or SS. New compared to Iversen and Seland (2002 and 2003) is that sulphuric acid gas is allowed to condense on the carbonaceous particles, thus creating aitken mode internally mixed particles of carbonaceous matter and sulphate.

Biogenic SOA is presently treated as OM emissions, although it is in reality a result of photochemistry in air initiated by biogenic emissions of volatile organics (terpene) from rural forests. The nature of the resulting biogenic (and also other) SOA particles is not well known (e.g. Henze and Seinfeld, 2006). Dentener et al. (2006) recommend condensation onto pre-existing aerosols. Since such a process would considerably increase the complexity of our look-up tables (Section 2.8), we have instead pragmatically assumed that the SOA is emitted with the same properties as OM, and is assumed internally mixed with BC when emitted in the same area. This is similar to organic particles emitted from biomass burning. Since huge forest areas are found in relatively pristine areas, initial nucleation and further condensation on the nucleated particles could indicate such behaviour.

The mineral dust and SS included in earlier model versions were prescribed diagnostically (Kirkevåg and Iversen, 2002; Kirkevåg et al., 2005), hence the new scheme is a considerable step forward in realism. Emissions of SS and DU depend in reality on wind speed, and DU is influenced by soil types and soil moisture. In the model, however, the emission sources of these components are fully prescribed as area-sources on the ground. The emitted size-distribution of SS is assumed to be three log-normal modes: aitken, accumulation, and coarse particles, while DU is only emitted as accumulation and coarse mode particles. A deviation from the emissions assumptions in Dentener et al. (2006) is our allocation of 2% of the SS mass from the coarse mode to the accumulation mode. This is motivated by the work of Mårtensson et al. (2003) who designed laboratory experiments to study particle production by bursting of air bubbles in saline water. They measured the number size distributions of the resulting aerosol as a function of dry diameter in the range 0.02–20 μm for different salinity, water temperature and bubble flux. Two dominant modes were identified; one centered at ca. 0.1 μm with the largest number of particles, and another at ca. 2.5 μm (see Fig. 6 in their paper). Our assumption is based on the dominant smallest mode found by Mårtensson et al. (2003).

2.5. *Aerosol physics and chemistry*

The sulphur chemistry is similar to Iversen and Seland (2002 and 2003) with a few extensions. We now calculate explicitly the DMS fraction converted into MSA following the method by Easter et al. (2004), who use the reaction rates given by Seinfeld and Pandis (1998). SO_2 is oxidized to sulphuric acid gas [SO_4(ga)] in clear air by OH, and to particulate sulphate in aqueous phase [SO_4(aq)] cloud droplets with efficiency determined by availability of H_2O_2, ozone, liquid water, and the rate of dynamic replenishment of cloudy air. We now include a chemical replenishment time of H_2O_2 of 1 hour in clouds, in addition to the replenishment time for cloudy air.

Sulphuric acid gas condenses on all particle surfaces available in a grid volume. When sufficient gas is available, a transfer coefficient defines the rate at which a mode of particles is changed to a mode with sulphate coating or mixing. The total number concentration of particles is not changed, but their size increases as particle mass is added and nucleation mode particles can be transferred to the aitken mode. For externally mixed BC in nucleation or accumulation mode, the condensation is one possible way to change from hydrophobic to hydrophilic. The changed size distributions of particle number and composition due to condensation are parameterized as described in section 2.8 below. The inverse of the condensation rate for a specific particle mode and type is the turnover-time of sulphur acid gas with respect to condensation on those particles. The condensation rates are calculated by equations for molecular diffusion of the sulphuric acid gas onto particles of given size and accommodation coefficient (see equations in Section 12.2 in Seinfeld and Pandis (1998)). The accommodation factors (see eq. 3 in Vignati et al., 2004) in this work are $\alpha = 0.3$ for insoluble particle surfaces and $\alpha = 1$ for soluble surfaces, also in accordance with Stier et al. (2005). The values of α are given together with the particle modal parameters in Table 1.

If the air in a grid square is sufficiently clean there can be a surplus of sulphur acid gas left during a model time-step after condensation has taken place. The entire surplus of this gas is assumed to create new externally mixed sulphate particles in the nucleation mode, with size parameters given in Table 1. Sulphur acid gas is not a historic variable in the model, since the chemically produced amount over a time step is immediately disposed of.

Coagulation is a process which reduces the number of particles whilst their total mass is conserved. In the model, we only take into account coagulation of nucleation and aitken mode particles with accumulation and coarse mode particles (see Fig. 1). Self-coagulation is only assumed to be efficient during the exhaust of some primary particles when particle concentrations are very large, and is accounted for in the direct emissions of accumulation mode SO_4 and BC. Atmospheric coagulation rates are calculated from equations on the Fuchs form for Brownian diffusion of small particles onto larger (see section 12.3 in Seinfeld and Pandis 1998). Coagulation of aerosol particles with cloud-droplets takes place when there is liquid water present in a grid square. Exclusively for the purpose of estimating the coagulation rates with cloud droplets, the droplet number concentration is prescribed as follows. In the four lowest model layers, the number concentration is 25 cm^{-3} over ice, 50 cm^{-3} over ocean, and 200 cm^{-3} over land. Above these four levels, the concentration is reduced to 25 cm^{-3} over ocean and 100 cm^{-3} over land. For small particles such as nucleation mode sulphate and BC, the in-cloud lifetime with respect to coagulation is about 1 hour, in agreement with suggestions by Ogren and Charlson (1983). The prescribed

droplet numbers used to estimate aerosol - cloud droplet coagulation rates, are quite similar to the calculated CDNC from the aerosols (see Figure 15).

2.6. Dry and wet removal

All compounds except DMS are both dry and wet-deposited. For dry deposition we use the same parameterization as Easter et al. (2004), which applies the resistance analogy of Wesely (1989) when calculating deposition of gases, and Binkowski and Shankar (1995) for dry deposition of aerosols. The dry deposition velocity thus depends on particle size, and the relative humidity influences this dependence for hygroscopic particles. Gravitational settling for coarse particles is included in addition to the turbulent exchange, but it is only applied in the lowermost layer in the model. Thus, we neglect downward gravitational settling from layers above. As deduced from the short SS lifetime of 0.19 d in Binkowski and Shankar (1995), Easter et al. (2004) (and thus also we) have a rapid dry deposition of coarse mode particles compared to other works, for example a median value of 0.4 in Textor et al. (2006).

An overview of all the wet scavenging and collection efficiencies is found in Table 2. Wet removal is parameterized the same way as in Iversen and Seland (2002), with an in-cloud scavenging coefficient defined as the mass fraction of the aerosol mode within the cloud droplet. The rainout is then determined by the local precipitation production rate. We only include scavenging by precipitation which contains liquid water. Although, some models include scavenging for cold ice-clouds (e.g. in Stier et al., 2005), we find the estimates too uncertain to include at present. Also, although the water-phase in CAM3 is parameterized to exist down to $-40\,^{\circ}$C, we have kept the same division between the water- and ice- phase precipitation as in CCM3 for scavenging of aerosols, which is a linear weighting between 0 and $-25\,^{\circ}$C. This scavenging assumption is the same as the optional sulphate parameterization in the standard CCM3 model (Barth et al., 2000), but slightly different than standard CAM3 sulphur cycle which uses $-20\,^{\circ}$ C as the lower limit (Collins et al., 2006a). We also include a crude parameterization for the fraction of cloud which is precipitating at any time inside a grid square with precipitation. For stratiform precipitation the fraction is set to 50% of the area below the cloud. The scavenging efficiency coefficients for sulphate and carbonaceous particles are results of a compromise between the values used by Iversen and Seland (2002 & 2003) for coagulated and chemically produced components, and by Stier et al. (2005) for the aitken mode. We assume that mineral dust has a hygroscopic coating.

For below cloud-scavenging we follow the parameterization in Seinfeld and Pandis (1998) (see in particular figures 20.11, 20.12, and 20.14, and associated text in that book). Below cloud scavenging produces washout from any atmospheric level through which liquid precipitation elements fall and collects the contaminants. Hence, contaminants inside clouds can be both subject to in cloud and below cloud scavenging. Collection efficiencies of falling elements depend on the size of the elements and the aerosol particles. The effective radius for rain-drops from convective clouds is assumed twice as large as for rain-drops from stratiform clouds. This follows from the standard Marshall-Palmer raindrop spectrum for increased precipitation intensity. Furthermore, convective clouds tend to have larger droplets even for the same precipitation rate (e.g. Rogers and Yau, 1989; Fig. 10.1). We have in consequence reduced the collection efficiencies with a factor 10, except for coarse particles.

Below-cloud scavenging rates are in principle independent of particle composition. Nevertheless, we have increased the rate for externally mixed BC compared to SO_4, simply because hydrophobic BC do not swell (see Table 2). The swelling effect is not taken explicitly into account in the connection with below cloud scavenging, but it is important in the humid conditions when precipitation is falling.

2.7. Parameterization of scavenging and transport in convective clouds

As shown in Iversen and Seland (2002), the transport and scavenging in convective clouds has potentially a large impact on both the vertical distribution and global columns of aerosols and precursors. These important processes are sub-grid scale in CAM-Oslo and in any model with horizontal resolution of a few km or larger. The convective mass-fluxes parameterized by Zhang and McFarlane (1995) in CAM3 (and CCM3) yields an efficient transport from the cloud base into the upper troposphere. An upward speed of only a few meters per second will empty a 1 km boundary layer over a time-step of 40 min. Updraft plumes only detrain in the model layers where they reach neutral buoyancy. In Iversen and Seland (2002) we omitted this vertical convective transport altogether, which lead to overestimated concentrations in the tropical boundary layer in particular. Concentrations in the free troposphere were probably underestimated, although observations of vertical concentration profiles are too few to confirm this. The impacts were studied in sensitivity tests and further by Iversen and Seland (2004), and in CAM-Oslo we include this transport.

As also studied in Iversen and Seland (2004) we also include mixing of constituents between updrafts and downdrafts inside the convective clouds. Downdrafts are produced partly by production of negative buoyancy when precipitation evaporates or by frictional drag from the falling precipitation. We pragmatically assume that shear-generated turbulence fully mixes the constituents between the updrafts and downdrafts. This considerably reduces the upward flux of boundary-layer constituents, see sensitivity test C2 below. The mass fluxes in both updrafts and downdrafts are calculated by the scheme of Zhang and McFarlane (1995) in CAM3, hence these transport calculations are done integrated with the parameterization of the convective clouds and the associated precipitation.

Finally, the scavenging by the convective precipitation is parameterized consistently with the convective transport assumptions. Thus, air in the boundary layer will be subject to in-cloud processing when drawn into the cloud from below, as well as to scavenging by falling precipitation from above. Hence, the contaminants will be taken up by cloud droplets which will rain-out according to the local precipitation production rate in the cloud, as well as be exposed to washout by falling precipitation elements from above. See Table 2 for values. We assume that all boundary layer constituents in grid squares diagnosed with deep moist convection is subject to this efficient precipitation scavenging. The process is tested in sensitivity test C1, where it is assumed that only air immediately inside or directly below clouds is exposed to scavenging. The boundary layer height is in this connection taken to be below η-level 0.90 pole-wards of 35 $^\circ$ latitude, and $\eta = 0.74$ equator-wards of 25 $^\circ$, and with a linear interpolation in-between.

2.8. *Size distributions, optical properties and cloud droplet number concentrations*

The aerosol module accounts for internal mixing between particulate matter of different physical and optical properties. Size distributed mass, composition, and numbers are re-constructed *a posteriori* from the available mass concentrations. Although all primary particles are assigned to consist of a superposition of log-normal distributions, the resulting size distributions are not. We modify the size distributions by the processes mentioned in section 2.4 using 44 size-bins in the radius range 0.001–20 μm and bin width $\Delta\log_{10}(r) = 0.1$.

An aerosol module which fully resolves size distributions is too expensive to handle by climate models, and simplified procedures are developed. The principles behind our procedures are described in Kirkevåg and Iversen (2002) and Kirkevåg et al. (2005), but they are extended because more aerosol processes are modelled in CAM-Oslo. The method is inspired by Chuang and Penner (1995). The aerosol life-cycle scheme (Fig. 1) calculates mass concentrations (or mixing ratios) of the chemical substances in the aerosols. As described in 2.4, each concentration field is tagged to processes as primary emissions, gas phase oxidation followed by nucleation or condensation, coagulation of nucleation- and aitken-mode particles on accumulation- and coarse-mode particles, or to aqueous phase oxidation. The physical and chemical processes influencing aerosol size distributions are exactly those tagging the concentrations.

With the tagged mass concentrations we re-construct the size distributed number and composition. In a grid volume there can be a range of size-distributed aerosol particles of different type which are externally mixed, and each can consist of internally mixed components. Each size-distribution is re-constructed from the production tagged concentrations starting with a superposition of up to four pre-defined log-normal distributions for each primary emitted or nucleated particle component. These distributions are moderated by solving the continuity equation for particle number and mass concentrations along the radius dimension. The processes accounted for are thus condensation, coagulation and aqueous phase oxidation. The hygroscopic property of each particle size and type are estimated by the volume mixing ratios, and water is added as function of relative humidity according to Köhler theory. For SS, mineral dust, sulphuric acid, SO_4 (ammonium sulphate) and BC, we use the same hygroscopic properties as in Kirkevåg and Iversen (2002), and for OM we apply the same hygroscopic property as in Kirkevåg et al. (2005).

The optical properties of each aerosol type and size are determined from Mie theory based on the complex refractive index calculated by the volume mixing rule for all aerosol components except BC. The Maxwell-Garnet mixing rule is subsequently applied to calculate the refractive index of the internal mixture of BC with any mixture of the other modelled components. BC is thus assumed only partly dissolved into a grainy structure when internally mixed. Integrating over the size distribution yields the spectrally resolved bulk aerosol optical properties (specific extinction, single scattering albedo and asymmetry factor). In addition, the concentration of activated CCN is estimated from the Köhler equation for given super saturations.

Wavelength dependent refractive indices for SS and SO_4 are based on Global Aerosol Data Set (GADS, Köpke et al., 1997; Kirkevåg and Iversen, 2002). As in Kirkevåg et al. (2005), OM has been given the refractive indices of the so-called WASO (water soluble) component from GADS, which was assumed to consist of various water soluble substances of mainly continental origins, such as the water-soluble part of OM. For BC we apply the refractive index given by Janzen (1979): m = 2.0 – 1.0i, assumed constant over wavelengths in the shortwave spectrum. According to Bond and Bergstrom (2006) the often used m = 1.74 – 0.44i (at 550 nm) is not representative for BC, while the reported higher values are the most promising. The value from Janzen (1979) is on the high side of the given range for various void fractions in Bond and Bergstrom (2007), but this is in the present work taken into account by assuming a BC mass density which is also on the high side, 2000 kg m^{-3}. The externally mixed BC of fractal structure has density of 507 kg m^{-3}. Assuming that the void in particles larger than the monomer radius (0.0118 μm) is filled with ambient air, the refractive index is calculated by the Maxwell-Garnett mixing rule, given the input refractive indices of compact BC and air (see Kirkevåg et al., 2005). The refractive indices for DU use values from Sokolik and Toon (1999) up to 0.57 μm, assuming a dust mixture of 99% quartz and 1% hematite. For longer wavelengths we use data from the station Solar Village in Saudi Arabia (Dubovik et al., 2002). The formerly used values from GADS gave excessive absorption, while the new refractive indices yield better agreement with retrieved single scattering albedo values from the AERONET (Dubovik et al., 2002).

Also the Mie and Köhler calculations are too expensive for climate modelling. Therefore, the calculations of optical

properties and CCN are tabulated for a large number of entry values of the process-tagged concentrations, relative humidity and super-saturation. Thus, the obtained look-up tables are used to estimate CCN and optical properties for arbitrary entry values. Interpolations between pre-calculated values in the look-up table for optical parameters are performed for each call to the short wave radiation code, which is once per model hour.

CCN concentrations are calculated from the look-up table every model time-step. In the present standard model version, we use presumed maximum super-saturations for a few basic cloud types: 0.10% in stratiform clouds, 0.25% in convective clouds over ocean and 0.80% in convective clouds over land (Kirkevåg et al., 2005). In any grid volume that is diagnosed with a positive cloud fraction from the cloud scheme, the CDNC is simply assumed equal to the CCN concentration. It is used to estimate effective droplet size for cloud optical properties and for auto-conversion to precipitation, and is thus central in the determination of the indirect effects of anthropogenic aerosols. In a further developed version of CAM-Oslo this crude assumption is improved by implementing the prognostic equation for CDNC described in Storelvmo et al. (2006), for which the CCN-production is a source term. A separate sensitivity test explores this new scheme.

CAM-Oslo applies a minor adjustment in the optics table look-up compared to CCM-Oslo (Kirkevåg and Iversen, 2002; Kristjánsson, 2002; Kirkevåg et al., 2005). A finer spectral resolution for visible light in the short-wave radiation code is used, which requires a minor change in the aerosol spectral bands. The 0.35–0.69 μm band in CCM-Oslo is in CAM-Oslo split into 0.35–0.64 and 0.64–0.69 μm, and the optical parameters are Chandrasekhar averaged over a set of finer resolved spectral intervals: 0.35–0.4, 0.4–0.47, 0.47–0.53, 0.53–0.57 and 0.57–0.64 μm.

Calculations of the Ångström parameter are based on AOD at wavelengths in the mid-visible (0.55 μm) and near-IR (0.865 μm), as in Kinne et al. (2006). Earlier versions of the look-up tables have been extensively validated (e.g. Kirkevåg and Iversen, 2002; Kirkevåg et al., 2005) by comparing explicit calculations of optical parameters, CCN and radiative forcing with the interpolated data from the look-up tables. An updated cross-validation for the new items in the latest version of the module remains to be done.

We calculate the radiative forcing due to the direct effect of anthropogenic aerosols as the difference in net short wave irradiance at the top of the atmosphere between the present (year 2000) and pre-industrial aerosol simulations, caused by scattering and absorption by aerosols. Since a major fraction of the aerosol mass is located at levels with similar temperature as the ground, the terrestrial long-wave contribution is neglected in this work (e.g. Charlson et al., 1992). Similarly, the radiative forcing due to the first indirect effect is calculated as the corresponding difference in calculated short-wave cloud forcing (SWCF) brought about by changes in the aerosol generated droplet number and size. In order to separate the forcing from the climate response in either case, the solar radiation scheme has to be called once for each effect in addition to the call with the standard parameterization which influences the atmospheric dynamics. We do not estimate a radiative forcing due to the second indirect effect, which in this work is a change in the lifetime of clouds due to reduced auto-conversion to precipitation in warm clouds.

3. Results

The presumed best aerosol model version has been run for 5 yr, using only the last 3 yr for statistics in order to establish quasi-stable aerosol climatology in both hemispheres and up to and including the lower stratosphere. At present CAM-Oslo is only run in a climate simulation set-up, that is without data assimilation or nudging of analysed meteorological fields. In order to get anthropogenic forcing from aerosols, each experiment is a twin simulation, one with present-day aerosol emissions and another with pre-industrial emissions. Both versions use present-day climatological sea-surface temperatures and greenhouse gas concentrations. Sensitivity tests are performed for year 5 with a 3-month spin-up, starting with aerosol concentration fields from the main simulations. The rather coarse resolution of T42 and 26 levels will cause some interpretation problems in areas with strong gradients. For example, and typically, near coastlines too high concentrations of SS must be expected at measurement sites within the same grid-square.

3.1. Budget and lifetimes

Annual mean sources, column burdens, residence times and sink processes are given in Table 3 for both the present day and pre-industrial emission estimates. The upper values in each row of the table are for present-day emissions. The residence time is given here as the ratio of the column burdens to the total sinks.

The total calculated SO_4 burden at 0.66 Tg S and a lifetime of 4.0 d is very close to the median mean value of 0.67 Tg and 4.1 d of lifetime given by the first AeroCom experiment (Textor et al., 2006). The SO_4 burden is noticeably higher than the value of 0.52 Tg found in Iversen and Seland (2002), in spite of lower emissions. A major part of this change is due to the strong increase in cloud-fraction in CAM3, and thus in CAM-Oslo, compared to CCM3 used by Iversen and Seland (2002 and 2003). Fig. 2 compares the zonally averaged cloud fraction in CAM-Oslo compared to CCM-Oslo. Except for low-level Arctic clouds that are discussed in section 2.3, the cloud-fraction is close to standard CAM as presented and discussed in Collins et al. (2006a). The larger cloud-fraction leads to faster oxidation of SO_2 to SO_4. Particularly striking is the increase in cloud fraction over tropical and subtropical regions, extending throughout the entire troposphere. The more efficient oxidation of SO_2 to SO_4 compared to Iversen and Seland (2002) is seen both in the loss of SO_2 due to aqueous phase production of sulphate

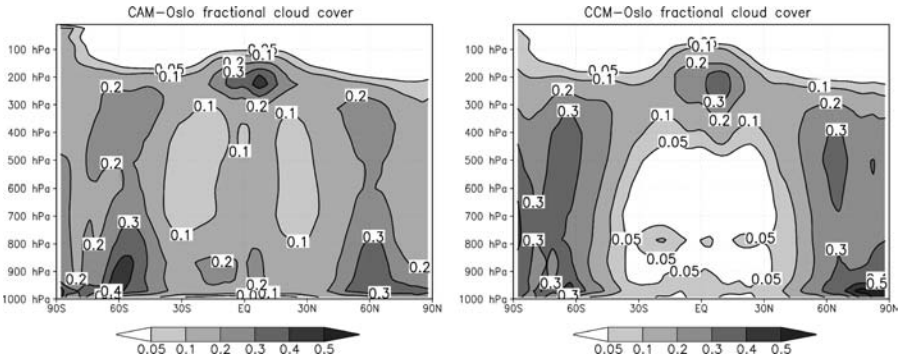

Fig. 2. Calculated zonally averaged fractional cloud cover in CAM-Oslo (left) and in CCM-Oslo (Kiehl et al., 1998; Kirkevåg et al., 2005) (right).

(59 versus 44%), and in the total lifetime of SO_2 (1.3 versus 1.6 d). The total column burden of DMS of 0.10 Tg is the same as in Iversen and Seland (2002). The emissions are somewhat lower in this work, but this is compensated by a smaller fraction yielding MSA. This fraction is calculated to 25%, while in Iversen and Seland (2002) the fraction was prescribed at 34%.

The global BC burden of 0.14 Tg is smaller than both in Iversen and Seland (2002) (0.16 Tg), and the median value in Textor et al. (2006) (0.21 Tg), although the residence time is now 6.7 d which is slightly longer than the model median (6.5 d) given in Textor et al. (2006). The lower column is thus a consequence of smaller global emissions. Similarly, the calculated global burden of OM is 1.30 Tg and the residence time 7.2 d, whilst the median values in Textor et al. (2006) are respectively 1.76 Tg and 6.2 d. The longer residence time of OM (7.2 d) than BC (6.7 d) in this work can partly be a consequence of the different geographical distribution of the BC and OM emissions. However, there are also differences in properties assumed for the emitted particles. Emissions of BC are dominated by biomass burning with only 1/3 coming from fossil fuel combustion. BC particles from fossil fuel combustion are externally mixed and hydrophobic, and with one exception they are smaller than the OM particles. The exception is that 10% of the emitted fossil fuel BC particle mass is assumed emitted as agglomerates shaped as fractals (see Section 2.4), with an equivalent size typical for the accumulation mode. Within the aitken particle size range, smaller particles (e.g. BC) have higher dry-deposition velocities than the larger (e.g. OM). Smaller particles also coagulate more rapidly with larger particles and cloud-droplets. Except for the fossil fuel BC agglomerates, this leads to a considerably faster transfer from insoluble to highly soluble accumulation mode particles than it takes for OM to change from low solubility aitken mode to highly soluble accumulation mode particles. For the initially hydrophobic fossil fuel BC, we calculate that 78% of the mass is transferred to the soluble accumulation mode with a turnover e-folding time of 1.0 d, and that 72% of the yield is due to coagulation. For biomass burning BC this coagulation yield is only 9%. In either case, the remaining part of the yield is due to condensation of sulphate gas. Due to the faster condensation process, the e-folding time for biomass burning BC is shorter than for fossil fuel BC: 0.8 d. These numbers are close to values found in other studies. Wilson et al. (2001) calculated 1.4 d turnover time due to condensation, and Stier et al. (2005) calculated a combined lifetime from condensation and coagulation of 0.7 d for purely hydrophobic BC and 1.1 d for insoluble OM particles.

The simulated SS burden is 5.8 Tg, compared to a median of 6.4 Tg in Textor et al. (2006). The calculated residence time of 0.27 d, however, is markedly shorter than their median of 0.42 d, and even shorter when compared to the model median of 0.6 d for the fixed aerosol source simulations (Textor et al., 2007). The short lifetime is mainly due to the dry deposition parameterization described in Section 2, but also because we use the suggested coarse mode log-normal size distributions of Dentener et al. (2006). As described in that work, the log-normal approximations have no size cut-off as opposed to the original bin distributions, thus giving a higher dry deposition than a bin model. The effect of the high dry deposition of coarse mode particles is also seen for DU, with a calculated burden of 10.4 Tg and a lifetime of 2.3 d. This can be compared with a median of 20.5 Tg and 4.0 d in Textor et al. (2006).

For the pre-industrial case, the DU and SS emissions given by Dentener et al. (2006) are the same as for present day emissions. We assume that all mineral aerosols are internally mixed and that the deposition is independent of the amount of condensate or coagulated matter on the mineral particles. The calculated burdens for DU and SS are thus the same as for present day. Compared to present-day, the pre-industrial emissions produce a 64% smaller SO_4 column burden. For carbonaceous aerosols the reduction is most pronounced for BC, which is reduced by 80%. Emissions of OM include SOA formed from terpene. The emissions creating SOA are assumed to be the same for both present day and pre-industrial cases. As a result, the estimated pre-industrial OM burden is about half of the present-day value. Furthermore, with no fossil fuel BC, hence no externally mixed hydrophobic BC, the lifetime and wet-scavenging

fraction for BC and OM are almost identical with pre-industrial emissions.

3.2. Mass and number distribution

Although many of the modelled particle types are internally mixed, we keep track of the individual mass mixing ratios of all the constituents. Figure 3 shows the annual mean burdens for each component as sum over all the modes. As expected from the relative short lifetime of SO_2, the maxima are found quite close to the source regions, both industrial and volcanic. However there is also a substantial export across dry areas, for example from Europe towards northern Africa, or from North America to the subtropical Pacific. In the case of SO_4 as well as for OM and BC, we still find the maxima close to the source regions, but the horizontal gradients are much weaker than for SO_2. The global DU burden is to a large degree dominated by the Saharan dust stretching out into the Atlantic, although a few other desert-like regions can also be traced in the column burden. Other source regions of DU are not included in the emissions, which, for example, can be seen in the low levels in North America and in culturally deforested areas. The SS burden reflects the emission patterns, although with somewhat lower gradients due to high precipitation and scavenging in major source areas, but also as a result of some transport into continental areas.

As shown in the AeroCom experiments (Textor et al., 2006, 2007), both the horizontal and vertical dispersion vary markedly from model to model. Models with high vertical transport or diffusion produce longer residence times for anthropogenic aerosols, since scavenging is less efficient in the upper portions of the troposphere. Figure 4 shows zonally averaged mass mixing ratios of SO_2 and the aerosol species. As opposed to in the results of Iversen and Seland (2002), where vertical contaminant transport by mass-fluxes in deep convective clouds were not taken into account (cf. Section 2.7), the aerosols are now distributed much higher into the troposphere. The results are therefore more

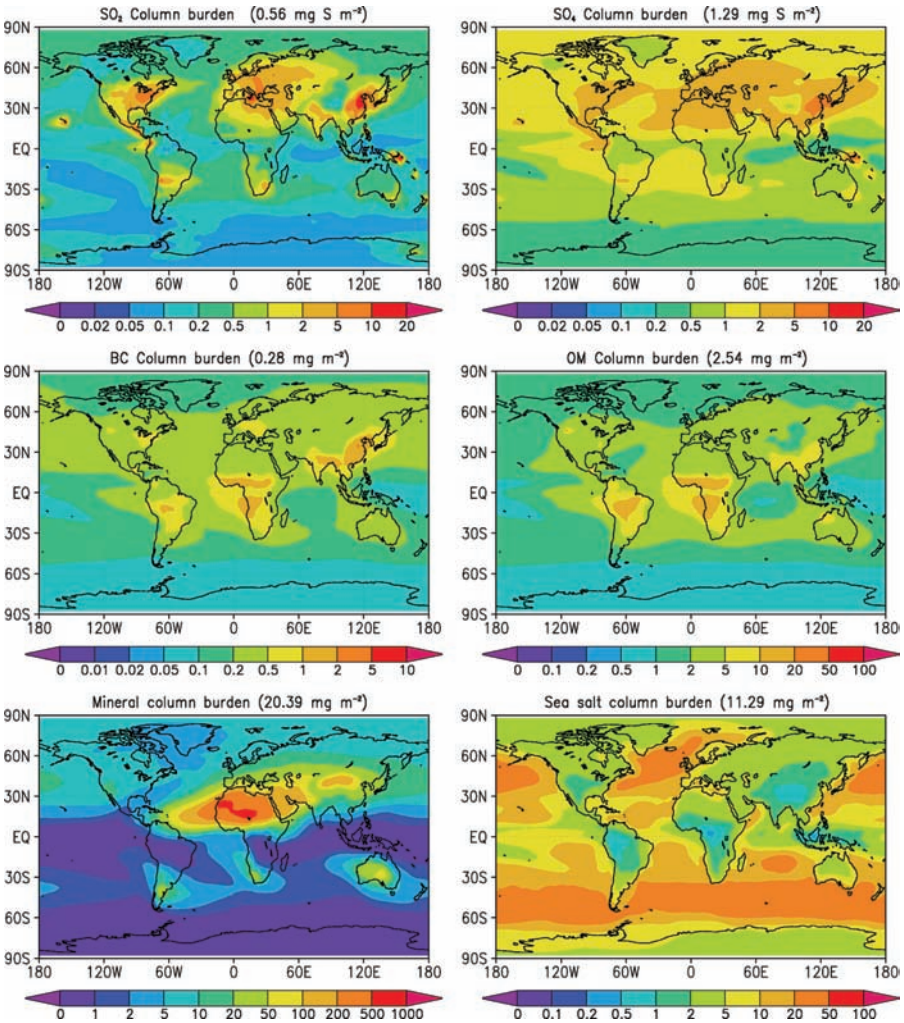

Fig. 3. Annually averaged vertically integrated mass columns of SO_2 and aerosol constituents in the control simulation. Unit: mg m^{-2}.

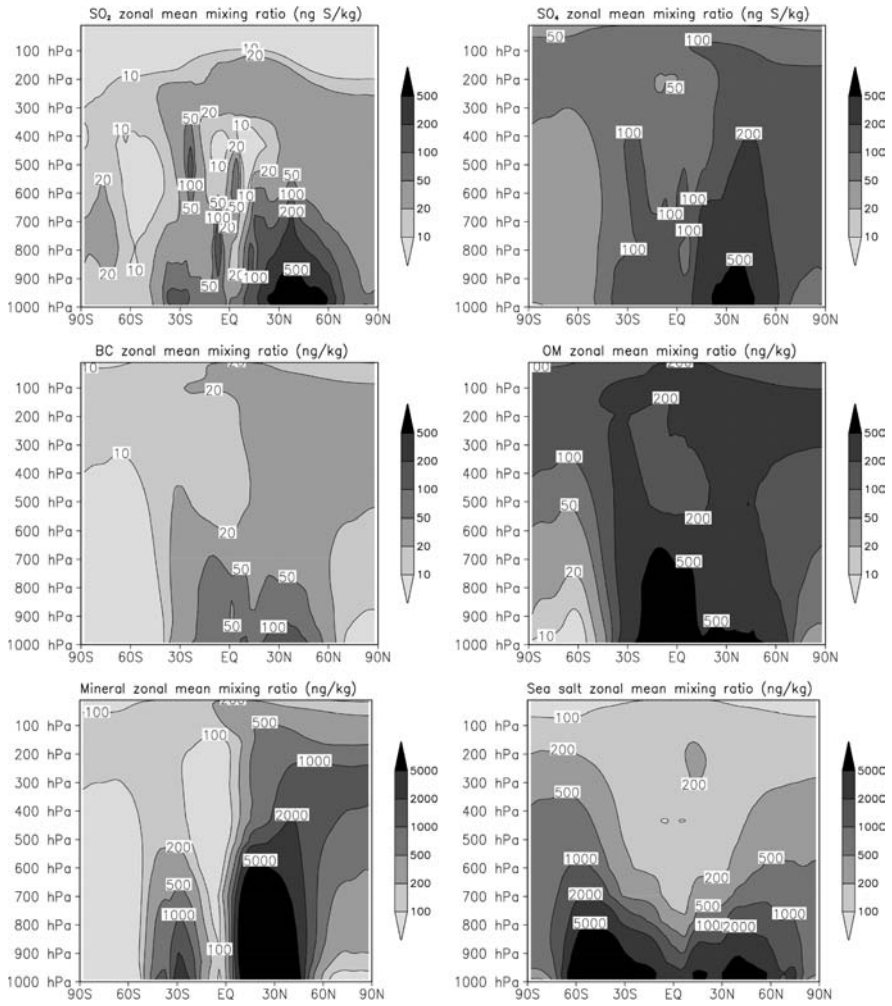

Fig. 4. Zonally averaged mass mixing ratios of SO_2 and aerosol components in the control simulation. Units: ng (S) kg^{-1} for SO_2 and SO_4 and ng kg^{-1} for the others.

similar to those of the model version which was submitted to AeroCom (Iversen and Seland, 2004; Kirkevåg et al., 2005; Textor et al., 2006) than to those of the original version (Iversen and Seland, 2002). There are considerable concentration levels in the middle and upper troposphere, whilst near the ground concentrations are reduced in areas with large convective activity, such as in the tropics. Since a large fraction of the mass of SS and DU are emitted from the ground surface in the coarse mode, the rapid dry deposition lead to a steep drop in mixing ratio with height. Notice that this also scavenges anthropogenic aerosols to the extent that these attach to coarse mode SS and DU (see Fig. 1). Even for mineral dust the modelled pattern is in many respects similar to that of sulphate, with a notable pole-ward transport in the upper troposphere. The deep convective vertical transport combines with an efficient horizontal transport in the middle and upper troposphere, and produces weak gradients in SO_4, OM and BC fields compared to for example Stier et al. (2005).

Although CCM-Oslo was amongst the models with efficient vertical mixing in Textor et al. (2006), it was no outlier in this sense. Textor et al. (2006) describes a number of explanations for the large variation in vertical mixing, and emphasize that different plausible parameterizations can give rise to a large diversity. We also note that the rapid reduction of SS with height is similar to the PNNL model also included in the model ensemble in Textor et al. (2006), and described in Easter et al. (2004) and Zhang et al. (2001). This is because CAM-Oslo applies the same dry deposition parameterization as PNNL.

We compare the modelled aerosol mass concentration of the lowest model level with a collection of surface measurements obtained by courtesy of AeroCom (http://dataipsl.ipsl.jussieu.fr/AEROCOM/). The measured concentrations span the years 1996–2002 and stem from sources like: Europe (EMEP: http://www.emep.int), North-America (IMPROVE: http://vista.cira.colostate.edu/IMPROVE/), the Atmosphere-Ocean Chemistry Experiment (Paul Scherrer Institute, by courtesy of

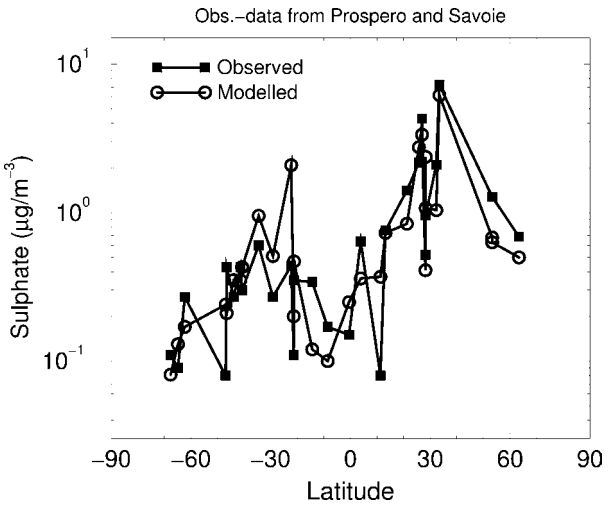

Fig. 5. Comparison of calculated and measured ground-level mass concentrations.: Sulphate in remote oceanic areas (measurements obtained from Prospero and Savoie, pers. comm.).

J. Prospero, University of Miami), and data compiled by the Global Atmosphere Watch (GAW) program. Since a climate model is not designed to match daily data, we compare with monthly or yearly climatological data by averaging concentration measurements over the entire measurement period. Figure 5 show yearly averaged SO_4 concentration for a number of remote sites. Figure 6 shows scatter plots for the observed and simulated monthly mean mass concentrations of all the aerosol compounds

Modelled concentrations of SO_4 over remote oceanic areas are in good agreement with the measurements. The difference in concentration levels between the two hemispheres as well as the tropical low concentrations is well reproduced. With regard to the AeroCom dataset, 76% of the modelled concentrations lie within a factor of 2 compared to measurements (657 out of 860 samples). There is a tendency to overestimate the concentrations at medium to high concentration levels.

Except for a minor fraction emitted as primary sulphate, the model calculated SO_4 is produced from oxidation of SO_2. To validate this process in the model, we need to compare the results for SO_2 as well as for sulphate. Figure 7 shows comparisons with measurements of SO_2 and SO_4 for a number of European and North American sites taken from EMEP and IMPROVE measurement network for the same period as in Figure 6. The model overestimates SO_2 over North America and to a lesser extent over Europe. We also find a smaller overestimate of SO_4 for the North American sites, whilst for the European sites the bias is negligible. Over both regions the model produces higher concentration of SO_4 than measured for intermediate concentrations. It is therefore possible that the chemical life-time of SO_2 is too high, in particular over Europe where we calculate slightly underestimated SO_4 near the source regions.

In the AeroCom dataset, concentrations of BC and OM are mostly taken from the North American IMPROVE network except for six stations for BC. We have also added a number of EMEP stations, both for BC and OM. As opposed to the IMPROVE stations only data from 2002 were available, within the chosen period of 1996–2002. The model clearly underestimates both BC and particular OM at many sites. The underestimate is most pronounced during northern hemispheric winter, in particular at European stations. For OM we therefore present comparisons with AeroCom (Improve) and EMEP in separate plots. Even though the EMEP stations probably are closer to locally polluted areas, the difference is larger and more consistent than expected. Too low emissions of OM over Europe, also excluding volatile organic compounds (VOCs), are a likely explanation. Another contributing aspect is the fact that the EMEP measurements include particle sizes up to PM10, while IMPROVE measures only PM2.5. Altogether 52%, the modelled concentrations fall within a factor of 2 of the measurements for OM and 56% for BC. The agreement over North America is better than expected, taking into account that the sources may vary significantly from year-to-year. The very limited geographical coverage of the measurement sites limits the validity of the comparison, however. Comparisons with retrieved AOD discussed in Section 3.3 reveal a significant underestimate of carbonaceous aerosols in areas affected by biomass burning. An overestimate of the wet-deposition is a likely cause, especially over ocean downwind of the emission areas.

SS mass concentrations compare well with high concentration stations, most likely marine sites. On continental stations near the coast the model strongly overestimate SS concentration. Altogether 41% of the simulated values lie within a factor of 2 of the measurements. At least a part of this overestimate can be attributed to the large grid size of the model, where a measurement station can be more than 200 km in-land while the emissions from the ocean fraction of the grid-box is distributed evenly across the whole area. Furthermore, the fixed emissions of aerosols and aerosol precursors are independent of the model meteorology. Possible connections between emission and loss-rates, that is strong wind both giving high emissions as well as high deposition, are therefore not accounted for.

The observation dataset for DU is not very large, but the large spread and strong tendency to underestimate the measured values point to uncertainties in the representation of dust. Only 15% of the values are within a factor of 2 compared to measurements. It is interesting to notice that Stier et al. (2005), who use a different emission scheme and a nudging of the meteorological data, find a very similar pattern when comparing their results to measurements. An obvious candidate for the underestimate is our assumption of a sulphate coating and rapid scavenging of all mineral dust particles. This hypothesis is supported by the fact that the model compares well with measured optical depths close to and downwind of the Saharan source regions, as discussed in Section 3.3. We note, however, that Stier et al. (2005) get a

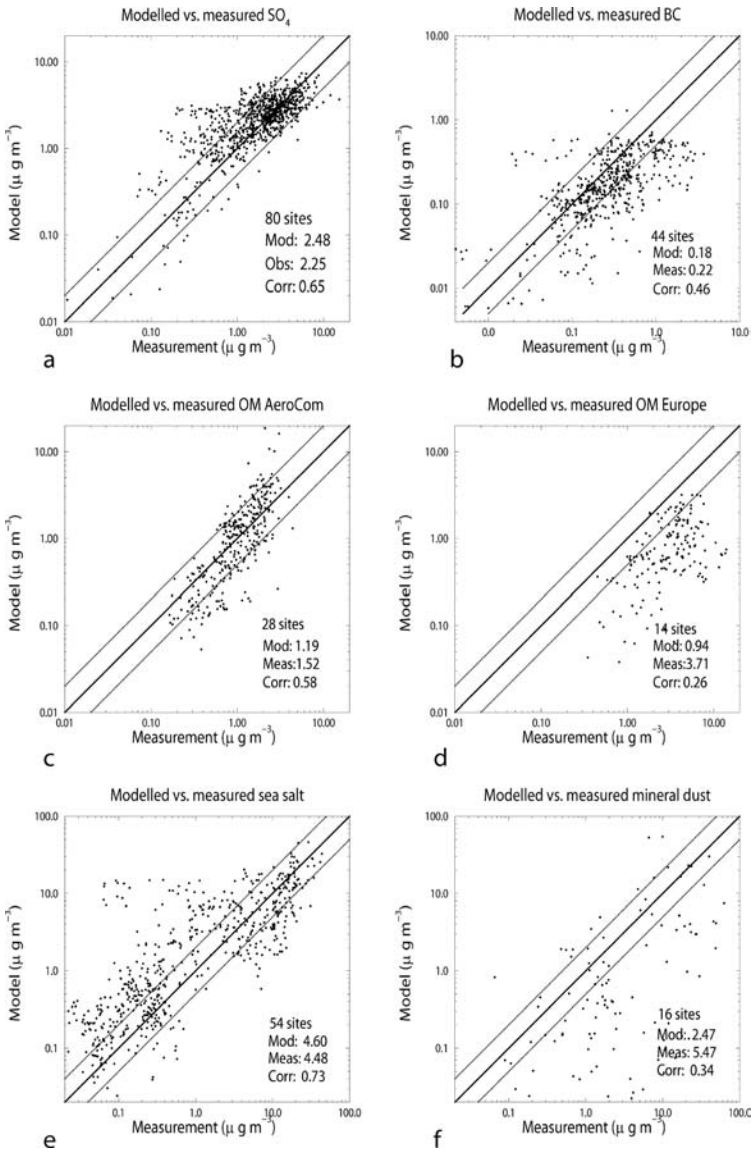

Fig. 6. Comparison of calculated and measured ground-level mass concentrations: Scatter plots for SO_4 (a), black carbon (b), particulate organic matter from the AeroCom intercomparison (c) and EMEP measurement campaign (d), sea-salt (e), and mineral dust (f). Measurements for 1996–2002 are made available through the AeroCom project from the AEROCE, AIRMON, EMEP, GAW and IMPROVE measurement networks. Units for sulphate is $\mu g(SO_4)$ m^{-3} and for other compounds μg m^{-3}.

similar underestimate despite their explicit differentiation between externally and internally mixed DU. An important possible candidate is therefore too small emissions, particularly for the Asian dust sources, which dominate large parts of the Pacific, as well as missing non-desert related emissions, for example from open agricultural fields.

Measurements of mass concentrations in the free troposphere are very sparse, and except for a few mountain peak stations, are generally found in short-term campaigns and usually only covering sulphur species. As seen in Iversen and Seland (2002 and 2003) the vertical distribution and global burden of sulphur species are sensitive to the treatment of convective transport and scavenging. This is very likely the case also for the other aerosol species. We advocate therefore that a validation of the vertical distribution of sulphur species to a large extent is a validation of the convective transport and scavenging and should be indirectly applicable for other aerosol compounds as well. The emission patterns are very different, however, and more measurements of vertical profiles are urgently needed. In particular one should focus on carbonaceous aerosols, since absorbing particles above clouds may efficiently reduce the planetary albedo. Lidar measurements which give the vertical radiative profile are promising, but have limited coverage in space and time.

In Figure 8 we present concentrations of SO_2 and SO_4 for four representative periods and sites of the Pacific Exploratory Mission (PEM). The data are taken from Barth et al. (2000), and were also used for model comparison in Iversen and Seland (2002 and 2003). The continuous lines represent model data from the standard simulation. The dashed lines are from a test on the convective treatment and are discussed in Section 4. In general,

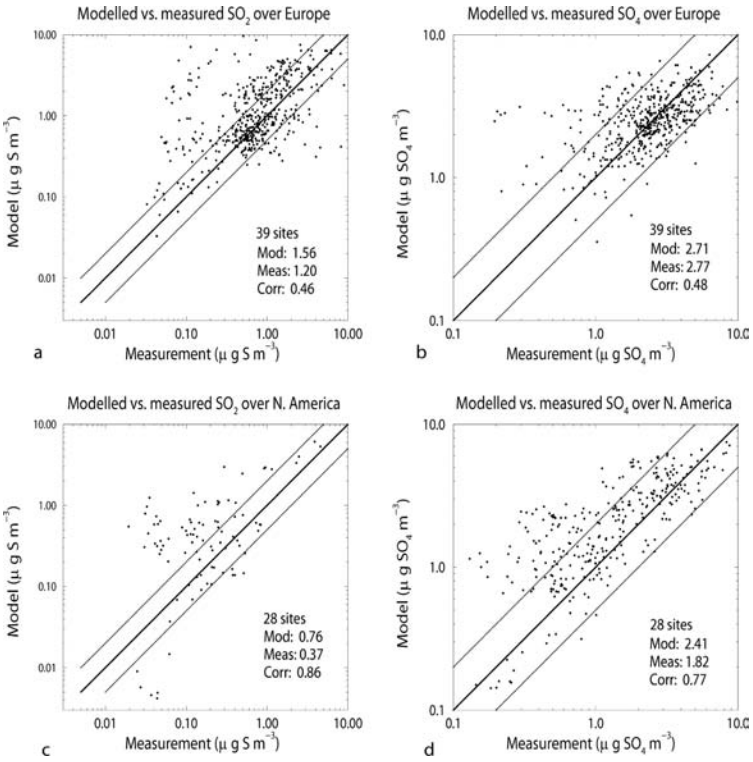

Fig. 7. Observed versus calculated yearly averaged SO_2 (a) – (c) and sulphate (b) – d) ground surface concentration in Europe (EMEP, upper panel), and in North America (IMPROVE, lower panel). Measurement period: 1996–2002.

we manage to regenerate much of the measured SO_2 profile, with a minimum in mid-troposphere, and a local maximum in the upper troposphere. The PEM grids given are quite large, typically $20 \times 20^\circ$, but since we do not know the actual flight-path, the model results are given as a grid average. The model underestimates the upper-level maximum, in particular over near continental sites in summer, for example the 'Hong Kong' sites. The spikes in modelled SO_2 in the lower troposphere are likely due to volcanic emissions close to or in the PEM grids. The volcanic emissions as well as the vertical distribution estimated by Dentener et al. (2006) are based on the year 2000, and may differ from the volcanic situation during the campaign. Hence, the deviations do not necessarily point to any deficiencies in the model. For sulphate the model compares well at low altitudes, but exhibits a strong overestimate in the upper troposphere. This implies that the modelled effect of scavenging and transport out of the boundary layer is reasonable, but with exaggerated transport. Our profiles follow very closely those of Barth et al. (2000). CAM-Oslo employs a similar approach to scavenging as used in that work, except for differences in the model boundary layer scavenging. While the boundary layer parameterization is important for the near-ground concentrations, the general approach to scavenging, assuming that it is proportional to the ratio between rain and total cloud-water, may have deficiencies, and calls for a closer study. A more indirect approach for checking the convective parameterization is to assume that the ground concentration is dominated by the convective transport and scavenging in remote areas with high convective activity. For this, we use observations obtained from Prospero and Savoie (personal communication) for sulphate in remote oceanic areas (Fig. 5). In Iversen and Seland (2002 and 2003), assuming no convective transport, the modelled value reaches 10 times the observed value in tropical ocean sites. The comparison in this work is generally quite good, except for one site in the southern hemisphere. The underestimate for the two northernmost sites is partly connected to the 50% reduction between the measured period and the year 2000.

While aircraft measurements usually give aerosol mass concentrations, the number concentration and the size range are important for validation of modelled concentrations of CCN or cloud droplet numbers. Vertically resolved measurements of aerosol number concentrations are even rarer than for mass. We have therefore chosen to compare our results with the model results from Stier et al. (2005), as well as three vertical measurements found in that work. Figure 9 shows zonal mean vertical distributions of aerosol number concentrations for the main modes as defined in Fig. 1. As opposed to Stier et al. (2005) we do not have any upper troposphere maximum in the nucleation mode. The overall much lower number concentrations in our model are to a large extent due to the assumed size of the sulphate nucleation mode particles (11.8 nm). In addition, the amount of SO_2 available for gas-phase oxidation in the upper troposphere may be too low in some areas. Figure 8 shows an underestimate in modelled SO_2 in the upper troposphere.

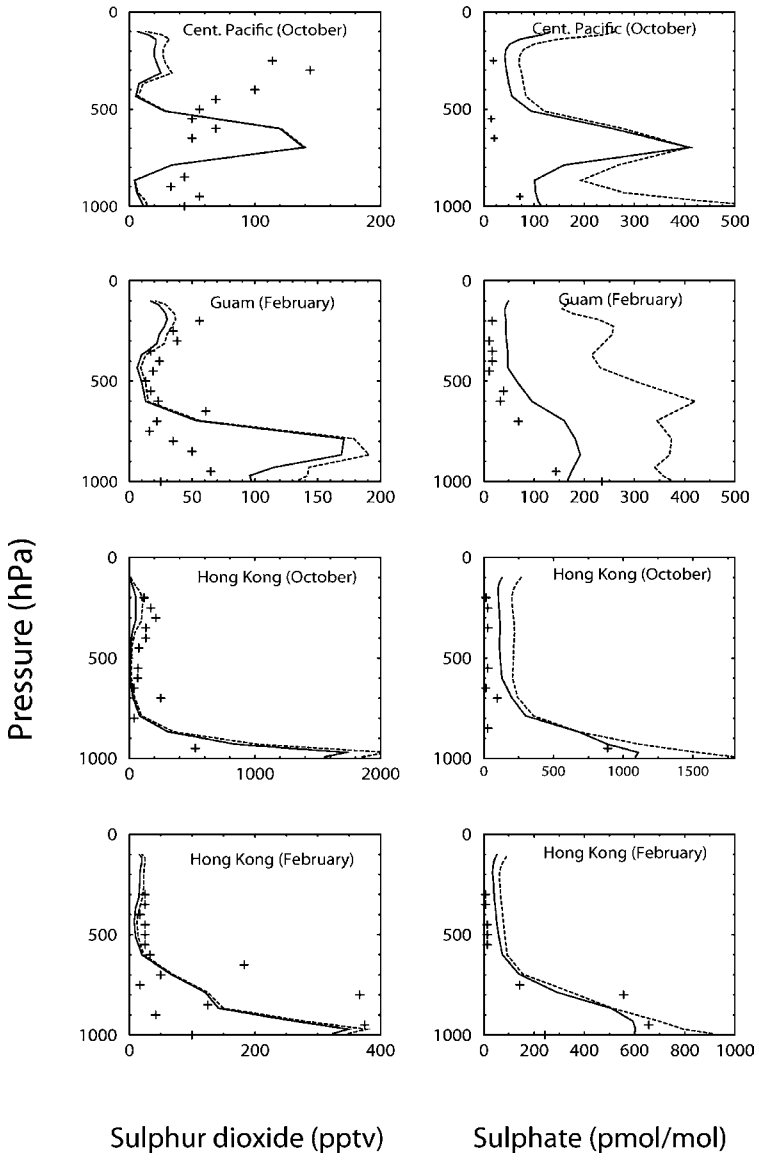

Fig. 8. Vertical profiles of SO_2 and SO_4 mixing ratios compared to flight measurements from the Pacific Exploratory Mission (PEM) over the period 1996–1999 presented in Barth et al. (2000). Data from each flight are given as two plots with SO_2 to the left and SO_4 to the right. Crosses denote measurements, continuous lines represent the standard simulation and dashed lines the sensitivity test C1 (see Table 4).

Furthermore, it is assumed that all sulphuric acid gas condenses on the available aerosol surface area inside the entire grid volume before any nucleation occurs.

The high concentrations of nucleation mode particles in Stier et al. (2005) are accompanied by higher concentrations of aitken and accumulation mode particles compared to our work. Our nucleation mode particles can grow to aitken mode particles after condensation of sulphuric acid gas. However, further growth by condensation into the accumulation mode is too slow to beat the coagulation with pre-existing particles in that size range. Hence, we only define a transfer of aitken and nucleation mode particles to accumulation and coarse modes by coagulation. The accumulation and coarse mode number is determined by the number of primary emitted particles within these size ranges. Note, however, that in the calculations of the look-up tables for optical properties and CCN activation, the aitken particles are allowed to grow to any size, provided there is sufficient sulphuric acid condensate available.

Until more free tropospheric measurements of aerosol numbers are available, it is difficult to validate the model with respect to particle number concentrations. Our results are quite close to representative vertical profiles of aerosol number concentrations given, for example in Seinfeld and Pandis (1998). Aircraft measurements reported in Stier et al. (2005) show somewhat higher values in the free troposphere with little height variation, and with number concentration reaching several thousands over Europe and over biomass burning areas. These measurements only count particles larger than 3 nm, however, meaning that the initial nucleation clusters are not accounted for. Virtually all of the particles modelled in this paper should be within the

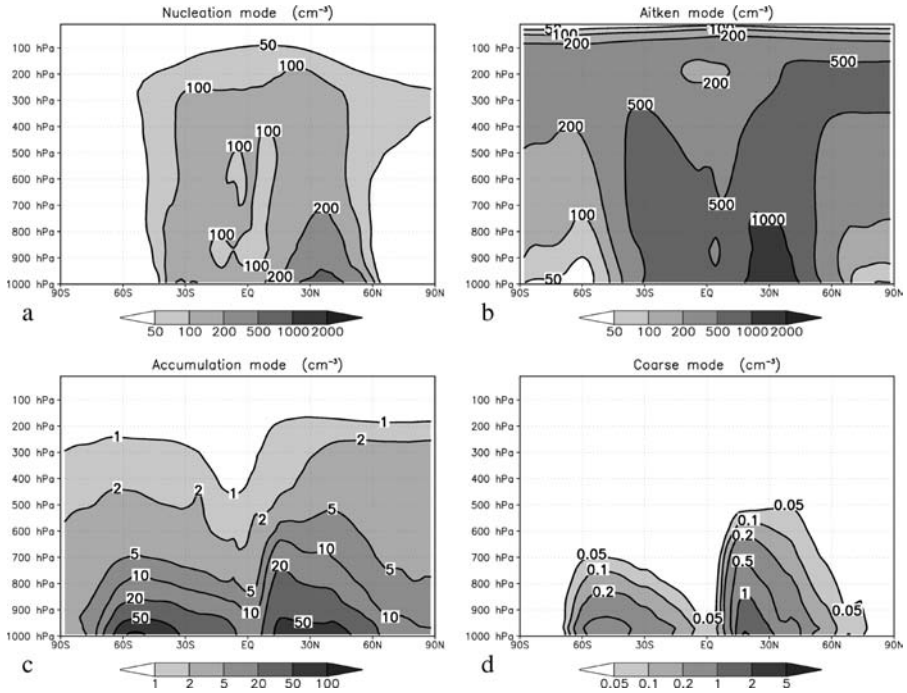

Fig. 9. Zonally averaged number concentrations (cm^{-3}) obtained using the definitions of aerosol modes given in Figure 1(a) the nucleation mode, (b) the aitken mode, (c) the accumulation mode and (d) the coarse mode.

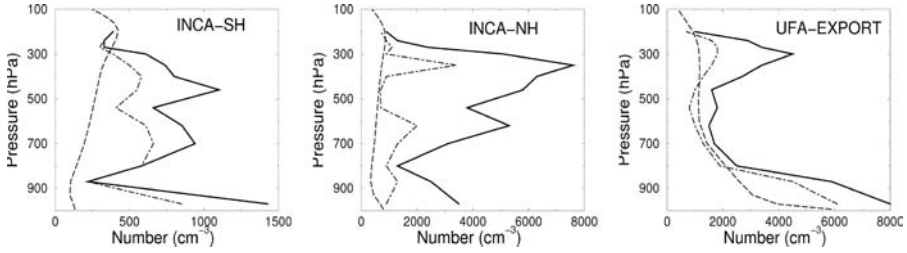

Fig. 10. Measured mean (solid lines), measured median (dash-dotted lines), and modelled mean (dashed lines) aerosol number concentrations for three flight measurement campaigns in the year 2000 over INCA-SH (Chile), INCA-NH (Scotland) and UFA-Export (Central Europe). Data are taken from Stier et al. (2005).

range covered by measurements. Figure 10 shows a comparison between modelled and measured aerosol number concentration for three campaigns. The model data is averaged over the given domain, and use the same period of the year as the measurements. The model number concentration in the free troposphere is to a large extent dominated by sulphate nucleation and aitken mode particles. The model generally underestimates the number concentrations over the two oceanic test areas, in particular in the middle and upper troposphere. The underestimate in the free troposphere is partly a result of our assumption of rapid coagulation growth of ultra-fine particles, although an underestimate of nucleation events can not be ruled out. The low-level model number concentrations, at least for the NH sites, are closer to the modelled median values, although more confined to the lowest model layer. In the SH case the model also underestimate the near ground concentrations. Possible explanations are nucleation of SO_4 particles in clean air, although aitken mode SS and biogenic aerosols can possibly make up a large part of the deficiency (Mårtensson et al., 2003; Lohmann and Leck, 2005).

3.3. Aerosol optical properties

As opposed to measurements of concentrations, numbers, and particle size, which require in-situ observations**, AOD** can be retrieved from some satellite instruments and used to evaluate the modelled AOD globally. We compare our results with combined MODIS-MISR-AERONET retrievals obtained from S. Kinne (personal communication). Liu et al. (2006) presented GISS model data, satellite retrievals and ground-based AERONET data averaged over land areas between 45° south and north, which we also use for comparison. Furthermore, we compare directly with the data from AERONET. In situ measurements are more

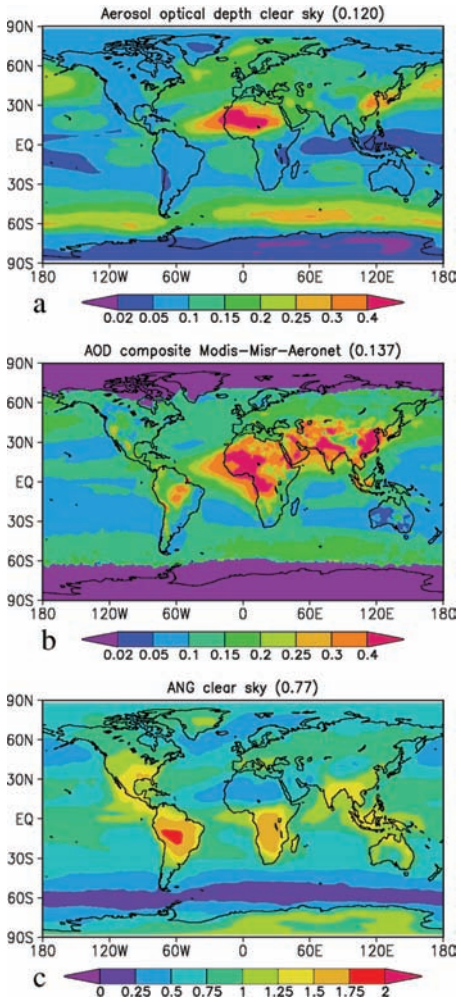

Fig. 11. Modelled and satellite retrieved aerosol optical depths (AOD) at 550nm. (a) Calculated clear-sky AOD, (b) Composite MODIS-MISR-AERONET AOD and (c) Clear-sky Ångström exponent (ANG).

exact than remote retrievals, but probably less representative for the optical properties over larger areas.

Figure 11a shows clear-sky AOD calculated by the model, and Fig. 11b the values from the combined retrieval. Clear sky values are found by weighting the all sky AOD by the cloud free area in each grid square and time step and dividing by the average cloud free area. The model calculated all-sky AOD (0.137) is notably higher than the clear-sky AOD (0.120). Both are quite close to the calculated AeroCom median all-sky value of 0.127. Data from a MODIS-MISR composite (Stier et al., 2005) give an AOD of 0.16, and globally averaged data from AERONET give 0.14 (Kinne et al., 2006). It should be pointed out that different satellite retrievals produce very different optical depths, in particular over land, although AOD values from satellite retrievals tend to be higher than both model values and AERONET retrievals (e.g. Liu et al., 2006). CAM-Oslo gives smaller AOD over oceans in tropical and temperate regions throughout the year compared to the GISS-model (Liu et al., 2006). The two models produce a similar seasonal cycle. The average clear-sky AOD in CAM-Oslo over the Northern Hemisphere in summer is 0.11. The respective number for the GISS model in Liu et al. (2006) is somewhat higher, 0.13, but the article does not reveal if it is for clear-sky or all-sky.

Judging by the satellite retrievals in Fig. 11b, CAM-Oslo simulates the AOD over oceans better than over most continental areas. The model gives slightly higher clear-sky AOD over southern polar and sub-polar regions than the retrievals. A possible explanation is that the SS emissions are not linked on-line to meteorological parameters influencing the emissions. The AeroCom sea salt emissions are based on global meteorological wind-speeds for the year 2000, and not from the winds calculated in CAM-Oslo. Large emissions are typically found in high wind speed regions, where also deposition processes are efficient.

Over continental areas, and in particular in areas dominated by biomass burning, CAM-Oslo seems to underestimate the AOD. Uncertainties in satellite cloud screening may partly explain this bias. The underestimate over biomass burning areas is also found when comparing with the AERONET site Los Fieros (see Fig. 13). Too low AOD are common amongst many global models (Kinne et al., 2006), but CAM-Oslo is in the lower range. A particularly large underestimate is found over the Indian Ocean and South Asia. This is probably caused by too much precipitation in the model (Hack et al., 2006). Overestimated precipitation probably also explain much of the too low AOD in tropical Africa, but precipitation biases can not explain the underestimate in South America. This may to some degree be due to under-prediction of the relative humidity in the biomass burning areas, which leads to too small hygroscopic swelling of the particles, although missing emissions can not be ruled out. For example Guyon et al. (2003) measure ambient relative humidities between 50 and 80% during the dry season, while CAM-Oslo averages at around 30–40%. It has also been suggested that satellite retrievals overestimate AOD over tropical rain forests in the non-biomass burning seasons, in particular over South America (Stier et al., 2005).

The reasons for the underestimate over temperate continental regions are probably more complex. We lack a number of possible aerosol compounds, such as nitrate, biogenic particles, non-desert mineral dust and anthropogenic SOA. Shortcomings in the simulations of the particle growth and the size distributions in general is another possibility, since for example our simulated mass extinction coefficient is rather low for sulphate, compared to the AeroCom median.

Figure 12a shows yearly mean values of modelled clear-sky versus measured optical depths for all the AERONET stations. As for the comparison with satellite measurements we see a notable underestimate in AOD also for comparisons with AERONET data.

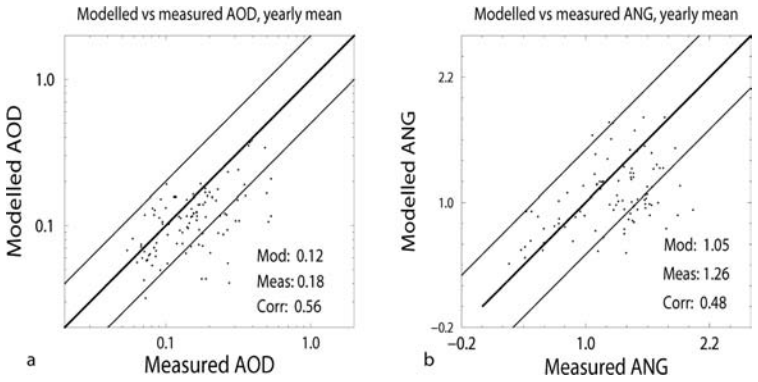

Fig. 12. Modelled versus measured clear sky aerosol optical depth at 550nm (left) and clear sky Ångström exponent (ANG) (right), yearly averaged. The measurements are from AERONET, cover the period 1996–2002, and are provided through the AeroCom project (Schultz et al., 2006).

Biases in optical depths may be connected not only to the amount of aerosol present but also to the assumed or calculated size distribution, refractive indices and hygroscopicity as well as relative humidity (see e.g. Kinne et al., 2006). The Ångström parameter, defined as

$$\mathrm{ANG} = \frac{\ln AOD_1 - \ln AOD_2}{\ln \lambda_2 - \ln \lambda_1},$$

where λ_1 and λ_2 denote the radiative wavelengths (0.55 and 0.865 μm, see Section 2.8), gives information on the column integrated aerosol size. Values larger than 1.5 indicate that aerosol optical properties are dominated by accumulation mode particles and smaller, whereas values smaller than 0.5 is typical of aerosols dominated by coarse mode particles (Stier et al., 2005). Simulated fields for clear-sky Ångström (ANG) is shown in Figure 11c. Clear-sky AOD is lower than the all sky values due to systematically lower relative humidities outside clouds. The drier clear sky conditions are also reflected in higher ANG due to less humidity swelling of hygroscopic particles. Maximum values are found in and near the biomass burning areas, and minimum values over remote ocean areas. The model produces a clear land–sea contrast, and the highest ANG values are mainly confined to tropical and subtropical areas. Although the satellite retrievals of ANG from MODIS over land to a large degree ignore coarse mode particle distributions (Stier et al., 2005), the modelled ANG values over northern temperate areas is generally lower than the retrievals. Data from all AERONET stations confirm a tendency towards a model underestimate (Figure 12b), but the sample spread is considerable. The outer lines indicate a deviation of larger than plus-minus 0.5, with 24% of the modelled values falling below the lower line, and only 6% above the upper line. The negative bias is mostly confined to mid- and high latitude sites, in particular in Northern Europe. Possible explanations include underestimated anthropogenic aerosol concentrations near industrial regions, and in particular for Europe, too much in-land transport of SS as described in section 3.2

The ANG values averaged over the subset of AERONET data presented in Liu et al. (2006) are similar to the values calculated in CAM-Oslo. CAM-Oslo reproduces these AERONET data closely, both with regard to seasonal cycle and amplitude, ranging from 0.96 in February to 1.26 in September. The satellite retrievals show no clear seasonal cycle, and a yearly average close to 1.25. The GISS AOD presented in Liu et al. (2006) were markedly larger and in better agreement with the retrievals than the CAM-Oslo AOD data. On the other hand, the GISS model yields little seasonal variation and an average ANG over land of only 0.6, which is about half of the CAM-Oslo value. Over oceanic areas CAM-Oslo produces a seasonal cycle in ANG with a minimum in NH winter of 0.75, and a maximum of 0.86 in September. These values lie between those found in two different MODIS retrievals (Liu et al., 2006).

A different way of looking at the data is by using single stations. Figure 13 compares the modelled and measured optical parameters at 6 different AERONET sites, each representing different aerosol regimes. Both oceanic sites, Ascension Island and Tahiti, compare reasonably well both w.r.t. AOD and size (ANG). One exception is the optical depth over Tahiti during southern hemispheric summer. Since the size compares well

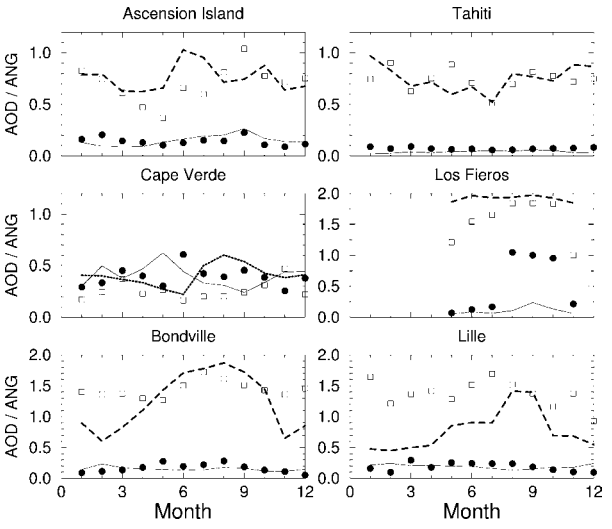

Fig. 13. Modelled and measured aerosol optical depth at 550nm (solid lines and black bullets) and Ångström exponent (ANG) (dashed lines and open squares) for a selection of AERONET stations for the period 1996–2002.

with the AERONET measurements even for different seasons, this suggest a general underestimate of aerosol burden during summer, possibly due to too efficient scavenging. Cape Verde, downstream of the Saharan desert also compare well, although with a somewhat different seasonal distribution. The biomass burning site, Los Fieros, shows a strong model underestimate during the burning season. The size is well represented, so the underestimate is likely to be due to underestimated emissions, too efficient scavenging, or a combination of both. As discussed previously, we note that the model strongly overestimates precipitation during the biomass-burning season in Central Africa, but we have no such verification for the dry season in South America. The two last sites share many of the same features, although one site is European, Lille, and the other, Bondville, is North American. The model has too many coarse mode particles relative to the number of fine particles (too small ANG) during winter. For optical depths, the yearly averaged measurements show a maximum during summer, while there is no discernible seasonal cycle in the model. While errors in aerosol burden and vertical variation certainly can not be ruled out, we believe, as discussed in Section 2.4, that we also lack a number of aerosol sources. In the case of Lille the proximity to ocean grid squares in the model also gives an unreasonably high column burden of SS during winter, reaching more than 50% of the total aerosol burden. A more realistic SS burden would likely have given an AOD underestimate also during winter.

3.4. Direct radiative forcing

The calculated global annual mean of the direct radiative forcing (DRF) at the top of the atmosphere (TOA), averaged over three years is $+0.02\,\mathrm{Wm}^{-2}$. As shown in Fig. 14a, negative DRF is confined mostly to areas with either low ground albedo and high sulphate to BC ratios, for example over eastern parts of North America and over the Mediterranean Ocean, or with relatively small amounts of low clouds, typically over biomass burning areas in the dry season. Positive DRF values are particularly pronounced over parts of south-eastern Asia, as well as at high latitudes in general. Schulz et al. (2006) report a range in DRF of -0.41 to $+0.04\,\mathrm{Wm}^{-2}$ for the ensemble of models participating in AeroCom. Our results are therefore in the upper end of the range. It should be noted that the present results are very similar to what was found for CCM-Oslo in the AeroCom comparison, both in terms of total number, $0.01\,\mathrm{Wm}^{-2}$, and horizontal distribution. The reason behind the positive forcing is a combination of several factors, discussed in Section 5.

As shown by Quian et al. (2006), the radiative forcing at the ground surface may have important consequences for the hydrological cycle. We find a ground forcing of $-1.18\,\mathrm{Wm}^{-2}$, which is quite close to the AeroCom average of $-1.02\,\mathrm{Wm}^{-2}$ reported by Schulz et al. (2006). The negative forcing for CCM-Oslo, referred to as UIO-GCM in that study, was $-0.84\,\mathrm{Wm}^{-2}$, which is markedly smaller than for the present CAM-Oslo. This can be attributed to the higher anthropogenic optical depth of 0.031 in CAM-Oslo, compared to 0.017 in UIO-GCM (Schulz et al., 2006). As seen from Fig. 14b, the surface DRF is most pronounced in eastern Asia, with values below $-5\,\mathrm{Wm}^{-2}$. Surface DRF values below $-0.5\,\mathrm{Wm}^{-2}$ are found over large areas of the globe, except parts of the tropics, in the Arctic, and south of 30 °S. In addition to the aerosol optical properties, the albedo of low clouds and the ground surface are important determining elements for the TOA radiative forcing.

3.5. Cloud droplet number concentration and aerosol indirect radiative forcing

Following the principles described in Section 2.8 we have calculated CDNC, cloud effective radii, and the first indirect radiative forcing. The first indirect effect is of anthropogenic aerosols is caused by increased numbers and reduced size of cloud droplets in non-freezing clouds. This is also called the cloud albedo effect, since it causes clouds to reflect solar radiation more efficiently. Figure 15 shows total and pre-industrial CDNC concentrations at model level $\eta = 0.87$ (typically 12–1400 m above ground), and as function of height, zonally averaged. As expected we find the highest CDNC close to the source areas of sulphur and carbonaceous aerosols. The CDNC calculated for the present-day case are similar to that calculated in CCM-Oslo close to the source

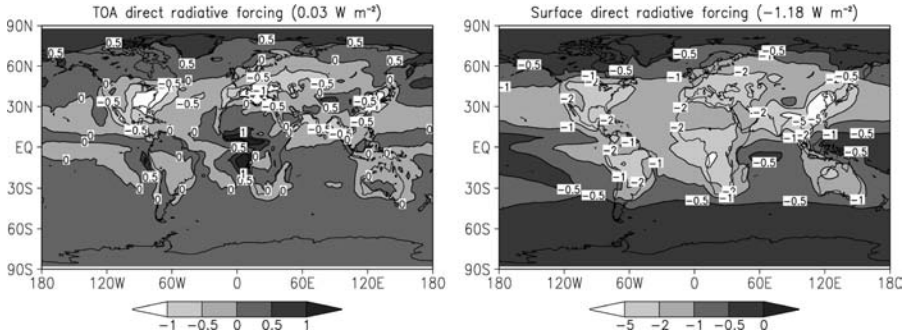

Fig. 14. Direct radiative forcing (Wm^{-2}) due to anthropogenic aerosols at the top of the atmosphere (left) and at the surface (right).

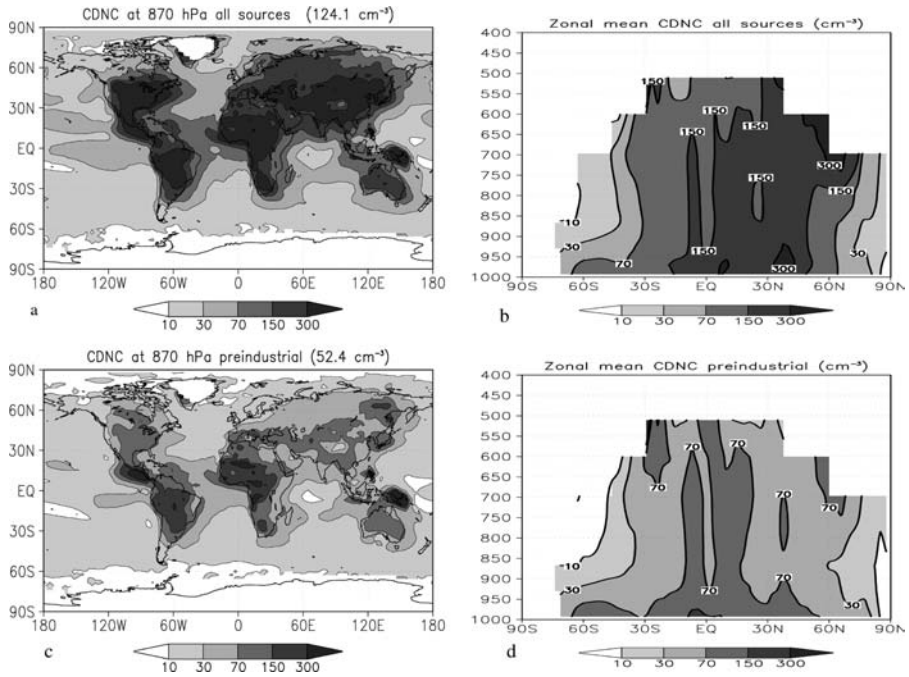

Fig. 15. Yearly averaged concentrations of cloud droplet number concentrations, CDNC (cm^{-3}-^{3}) at model level $\eta = 0.87$ (a) and (c) to the left) and zonally averaged (b) and (d) to the right) for present day (upper panels) and pre-industrial (lower panels) emissions.

regions, but with a strong reduction over ocean, reflecting the reduction in SS particles.

Despite the low number of cloud droplets over ocean the model compares reasonably well with cloud droplet effective radii as would be seen from satellite, retrieving the droplet effective radii from the model in a similar way to a satellite retrieval from the atmosphere. This can be verified by comparing Fig. 16 with similar figures in Han et al. (1994) and Kirkevåg et al. (2005). See also Kristjánsson (2002). Over tropical ocean areas the model gives the same maxima of 14 μm as the satellite retrievals, although not all the time in the same geographical areas. The model overestimates the effective droplet radii over the Southern Pacific Ocean by 1–2 μm, indicating that the model either underestimates the CDNC or overestimates the liquid water content in pure SS /biogenic sulphate conditions. Over land, in particular away from the tropical regions the model markedly overestimates the effective droplet radius compared to satellite. Missing aerosol components, such as nitrates, secondary organics, some soil components, and primary biological particles (Jaenicke, 2005), is probably contributing to this. Hence, both pre-industrial and anthropogenic aerosol components are missing, which was also seen in the comparison of aerosol mass concentrations of selected species with measurements.

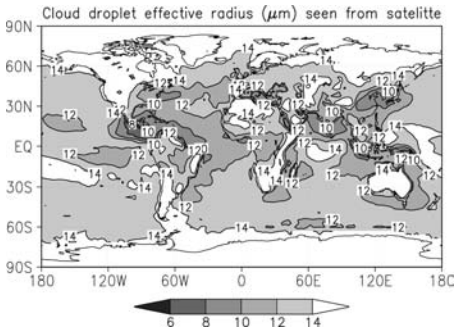

Fig. 16. Cloud droplet effective radii (μm) as seen from satellite for comparison with satellite retrievals according to Han et al. (1994) and presented in Fig. 6 in Kristjánsson (2002).

The pre-industrial case has a very low number of cloud droplets at $\eta = 0.87$, reaching more than 100 only in biomass burning areas. As seen from the vertical profiles in Figure 15, there is a strong vertical gradient at southern hemispheric mid-latitudes. We do not have measurements of CDNC dating back to pre-industrial time, but measurements of CDNC over clean continental conditions typically give values from 100 to 500 cm^{-3} (Ghan et al., 1997). Hence, we believe that we underestimate CCN concentrations from natural sources. The indirect effect is somewhat limited in strength by use of the prescribed lower and upper limits for cloud droplet radii of 4 and 20 μm in the Slingo (1989) scheme for shortwave radiative properties of cloud droplets in CAM3.

The low number of background aerosols together with overall large effective radii yields a large first indirect effect and a global TOA forcing of ca. -1.8 Wm^{-2}. The geographical pattern in Fig. 17 largely follows the anthropogenic aerosol distribution, with (negative) maxima of more than -5 Wm^{-2} over industri-

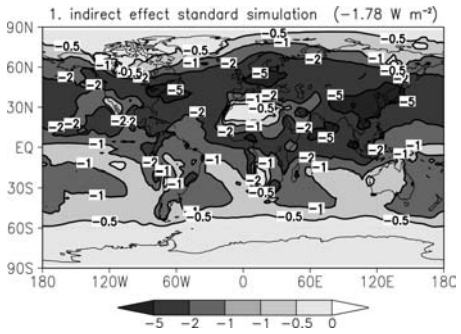

Fig. 17. Calculated first indirect radiative forcing (Wm^{-2}) for the control simulation.

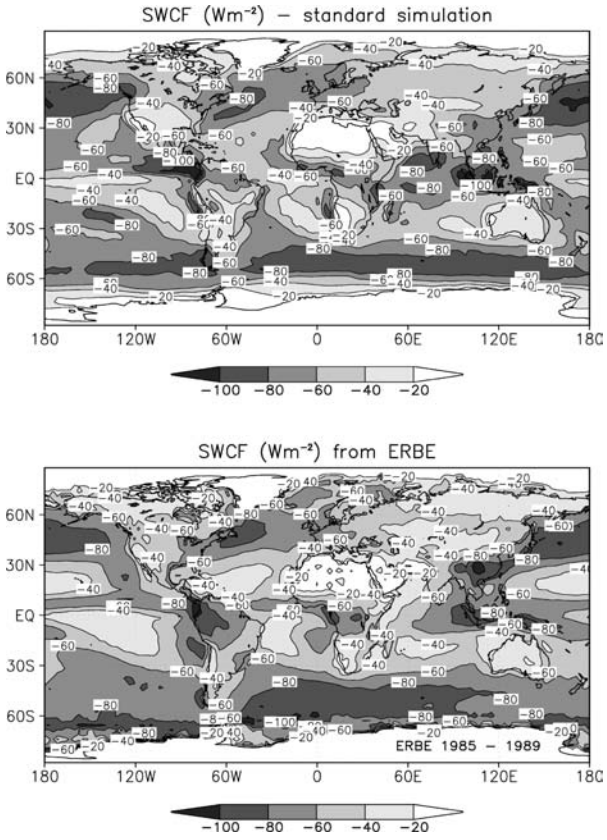

Fig. 18. Short-wave cloud forcing (SWCF, unit W m^{-2}) in the control simulation (upper panel) and from the Earth Radiation Budget Experiment (ERBE,1985–1989) (lower panel).

alized areas and $-2\,Wm^{-2}$ over biomass burning areas, but is considerably smoother with values just below $-0.5\,Wm^{-2}$ over the Southern Pacific Ocean. The first indirect TOA forcing in CCM-Oslo was $-1.1\,Wm^{-2}$ using prescribed mineral and SS aerosols, whilst the indirect effect of CAM-Oslo is close to the upper bound referred to by Lohmann and Feichter (2005). A similar difference is seen for the second indirect effect, which is the cloud life-time effect. Kirkevåg et al. (2008b) used the present CAM-Oslo coupled to a slab ocean and found a 30% larger effect than in CCM-Oslo. Lohmann et al. (2000) related the indirect radiative forcing to the CDNC, and thus to the number of aerosols available for activation, in the background pristine atmosphere. They showed that reducing the minimum CDNC from 40 to 10 cm^{-3} increased the negative global indirect aerosol forcing from $-1.1\,Wm^{-2}$ to $-1.9\,Wm^{-2}$. A similar experiment in Kirkevåg et al. (2008b) gave a 40% reduction in the combined first and second indirect effect when CDNC was increased by 15 cm^{-3} everywhere. As discussed by Storelvmo et al. (2006) and shown in Section 5.1 below, more elaborated calculations of CCN activation and CDNC aging is also likely to reduce the estimated indirect effect.

The model-calculated total SWCF is shown in Fig. 18. The figure also shows retrieved satellite data from the Earth Radiation Budget Experiment (ERBE) for comparison (Harrison et al., 1990; Kiehl and Trenberth, 1997). Globally averaged short-wave cloud forcing (SWCF) with present-day emissions is in CAM-Oslo estimated at $-55.1\,Wm^{-2}$, close to $-54.7\,Wm^{-2}$ in CAM3 (Collins et al., 2006a) and in acceptable agreement with $-54.1\,Wm^{-2}$ from ERBE. The agreement is good, also for broad regional characteristics. Considerable deviations are seen in tropical South America where the SWCF is underestimated. Differences are also seen over the subtropical Pacific Ocean and the Indian Ocean with slight overestimates. The excessive cloud cover, LWP, precipitation and in turn also the cloud forcing over the western Indian Ocean, are related to deficiencies in the Zhang McFarlane scheme closure assumptions in CAM3 (Hack et al., 2006).

4. Sensitivity tests

As shown in the AeroCom project and related experiments, the diversity among global aerosol modelling results are considerable, both for aerosol mass, optical properties, and direct and indirect radiative forcing. Furthermore, use of harmonized emissions hardly reduces the spread, and the diversity is similar for basic variables (concentrations) as for the forcing (Textor et al., 2007).

To test some of our assumptions and parameterizations we have conducted eight sensitivity tests. Technically the tests are set up for year 5 starting in October the year before, with initial aerosol fields from the standard simulation. Hence, each test has 3 months spin-up, and results for the final 12 months are compared to year 5 of the original run. As in the standard simulation, each test is run both with present-day and pre-industrial emissions, enabling us to discuss the sensitivities of parameterizations both on the aerosol budgets and their effects on the radiation budgets.

The tests are grouped into two subclasses. The first class of tests (C1–C4) investigates parameterizations of transport and scavenging in deep convective clouds, and the parameterization

of formation of rain by auto-conversion. The second class (S1–S4) addresses the assumed primary particle size distributions and speciation within the four main particle modes. An overview of all the experiments is given in Table 5, and a summary of aerosol column burdens and lifetimes for all the tests are given in Table 6. The effects on AOD, cloud droplet properties, and direct and indirect radiative forcing are found in Table 7.

Test C1 investigates the effect of our assumption that contaminants in the entire boundary layer below convective clouds are available for scavenging as described in Section 2.7. When allowing scavenging only to take place within the local cloud fraction, we get less scavenging of both SO_2 and aerosols near the ground, and hence more material available for convective transport and dry deposition. As seen from the comparisons with vertical measurements of SO_2 and SO_4 in Fig. 8, we also get higher concentrations in the upper outflow levels of convective clouds. The high concentrations of SO_4 found in this test both in the upper troposphere and near the ground are not reflected in the measurements as presented in Fig. 8. The effect on the column burden is strongest for SO_4, with an increase of close to 40% both with present-day and pre-industrial emissions, with somewhat lower values for BC and OM. For SS on the other hand, we find an unchanged (or a very small decrease in) column burden compared to the standard simulation. The reason for this is the very swift dry deposition of coarse mode particles due to gravitational settling. The reduced convective scavenging in this test yields a higher fraction available for dry deposition.

The increase in column burden is reflected in a 35% increase in anthropogenic optical depth. The effect on the TOA DRF is a significant drop from 0.03 to $-0.06\,\mathrm{Wm}^{-2}$. Due to the strong increase in optical depth, this test yields the largest absolute ground forcing, $-1.55\ \mathrm{Wm}^{-2}$. The shift from a slightly positive to a negative DRF is caused by an overall increase in anthropogenic scattering extinction in the middle and upper troposphere, while the extinction by absorption increases slightly in the upper troposphere and decreases at high latitudes in the mid-troposphere. This is reflected in an increase in vertically integrated SO_4 mass which is almost twice that of BC (see Table 6). The larger increase in SO_4 than BC is partly due to an increase in sulphate pre-cursors (SO_2), but also due to the efficient dry deposition of fine mode BC particles. The higher aerosol concentrations in the lower troposphere are also reflected in an increase in CDNC of more than 35% (at $\eta = 0.87$), both for present-day and pre-industrial emissions. Due to the higher cloud droplet numbers also in the pre-industrial case (cf. Lohmann et al., 2000), the increase in indirect radiative forcing is relatively small (from -1.78 to $-1.88\,\mathrm{Wm}^{-2}$).

In **test C2** we assume that there is no mixing of the constituents between convective updrafts and a downdrafts. We find a 20–25% increase in column burdens for sulphate, OM, and BC, and somewhat smaller increases for the coarser SS and mineral dust particles. The lowest starting point of the downdrafts is in the mid-troposphere, and noticeable changes are only found above this level. The difference in aerosol mass mixing ratio between C2 and the standard simulation increases with height toward the upper troposphere and lower stratosphere, where it is twice as large as in the standard simulation. The increase in carbonaceous aerosols in the upper troposphere causes enhanced absorption and increased positive contributions to DRF, which increases to $0.09\,\mathrm{Wm}^{-2}$. As in test C1, the increase in anthropogenic column burden and optical depth has a strong effect on the ground forcing ($-1.52\,\mathrm{Wm}^{-2}$), while we find only a small increase in the aerosol indirect effect ($-1.84\,\mathrm{Wm}^{-2}$).

Test C3 investigates the effect of the Freeze-dry cloud-parameterization. It is found to have generally little impact on the aerosol column burden and radiative effects. The largest change w.r.t. column burden is a 2% increase in mineral dust, compared to the standard simulation. Despite an increase of 20–30% in low cloud fractions over large areas of the Arctic, the change in burden is mainly found over sea-ice during winter, where wet scavenging is of less importance.

Test C4 investigates the effect of changing the parameters for auto-conversion back to their original CAM3 values (cf. Section 2.2). We get 21% less cloud water in C4 than in the standard simulation. Lower liquid water content implies a more efficient in-cloud scavenging, given that the precipitation release rate remains approximately unchanged, and this turns out to be the case. In result we get a minor overall reduction in aerosol burdens, ranging from 1% for BC to 5% for SO_4. The reduction in optical depth is actually larger than the change in any of the column burdens. This is because auto-conversion only takes place in warm clouds. Hence, the aerosol reduction is encountered in the lower portion of the troposphere, where relative humidity is high and consequently the water-uptake in the particles is large. The number of cloud droplets is almost unchanged from the standard simulation, but due to lower liquid water contents we get an overall reduction in droplet size. Anthropogenic changes in CDNC and effective cloud droplet radii are actually slightly smaller than in the control simulation but less liquid water implies an enhanced sensitivity to changes in CDNC and effective radius (see e.g. Kiehl et al., 2000). C4 produces the largest indirect effect of all the sensitivity tests ($-1.96\,\mathrm{Wm}^{-2}$).

In **test S1** the emitted size distribution of SS particles follows the recommendation by AeroCom (Dentener et al., 2006). Hence, the 2% of the originally assumed coarse mode SS emissions, which was re-defined to the accumulation mode in the standard run, is now taken as coarse mode particles. Although the total emitted mass is the same, the mode shift is found to have a considerable effect on the aerosol optical depth. The SS column burden is reduced by close to 10%, and the total AOD with 22%. The largest changes are found in the sub-polar southern hemisphere with reductions exceeding 40%. The reduction in SS column burden is a result of the much shorter life-time of the coarse mode (0.2 d) due to gravitational settling than the accumulation mode (1.6 d). The stronger decrease in aerosol optical depth than in column burden is caused by the shift to

larger particles, leading to a reduced mass extinction coefficient from 6.3 to 3.7 m^2g^{-1}, which is close to the AeroCom median of 3.0 m^2g^{-1} reported by Kinne et al. (2006). The reduced SS number concentrations are also reflected in CDNC near the ground. The number of cloud droplets is reduced less than the reduction in the number of accumulation mode SS particles. One reason can be that not every accumulation mode SS particle is activated as CCN, but also that the number of SO_4 aitken mode particles is increased. A reduced surface area of SS particles available for condensation of sulphuric acid gas leads to a rise in SO_4 nucleation. The overall reduction in CDNC together with increased anthropogenic changes in CDNC and cloud effective radii produce a strengthened indirect effect of $-1.95\,Wm^{-2}$.

The opposite result pattern is found in **test S2**, in which 0.1% of the coarse mode emissions of SS is shifted to the aitken mode. The increases in column burden and optical depth are only 0.3 and 1.1% respectively, although the globally averaged number of SS particles in the lowest model layer increase by 4.2% for present day and 8.9% for pre-industrial emissions. The increase is highest over pristine background areas, where very low cloud droplet numbers are found in the standard simulation. Despite a strong increase in SS aerosol number concentrations, the CDNC increases much less. This is partly because not all the particles are activated, but also because the shift towards smaller particles reduces the number of activated SO_4 aitken mode particles. The reason for this is increased competition between SS and SO_4 particles for available SO_4 condensate.

Although we find larger anthropogenic contributions to CDNC and effective cloud droplet radii in S2 than in the standard simulation, the overall increase in cloud droplet numbers lead to a somewhat smaller indirect radiative forcing ($-1.71\,Wm^{-2}$). The surface DRF is also relatively modestly changed in this test ($-1.12\,Wm^{-2}$). The increased SS surface area decreases the amount of SO_4 condensate on BC particles, which reduces the size of absorbing particles and thus the aerosol absorption efficiency.

Test S3 investigates the sensitivity to the assumed emitted size distribution of primary sulphate, by emitting it in stead as sulphuric acid gas. This increases the SO_4 column burden by 1%, but due to the implied reduced size of SO_4-containing particles, the total aerosol optical depth is reduced by 1% and the anthropogenic optical depth by 3%. Since the primary emissions of SO_4 are dominated by fossil fuel sources, we find much larger impacts regionally, with a reduction in total optical depth of more than 15% over central Europe and 10% over North America. Since many of the ground surface measurements are near industrialized areas, the assumed size distribution for a minor part of the total burden may strongly influence the validation of the models. The reduction in accumulation mode particle numbers reduces the scattering of SO_4. We therefore find a slightly higher, that is a more positive, direct effect in this test. The effect of S3 on CDNC consists of two competing effects, one from the reduction in number of accumulation mode particles, and the other from increased nucleation and subsequent formation of aitken mode particles. The net effect on the indirect radiative forcing is small.

Both classical aerosol theory and aerosol measurements indicate that the fraction of aerosols in the accumulation mode should be higher than found in this work (see for example Seinfeld and Pandis, Ch. 7, 1998). **In test S4,** we assume that emissions of internally mixed BC and OM particles from biomass burning go directly into the accumulation mode in stead of the aitken mode. We then find a strong reduction in the simulated burden of carbonaceous particles, caused by enhanced in-cloud scavenging rates. The decrease in aerosol burden is larger than the increase in the mass extinction coefficient, resulting in somewhat lower optical depths. The effect of the reduction in carbonaceous aerosols on DRF at TOA is striking, since this test yield the strongest negative TOA DRF ($-0.07\,Wm^{-2}$). The lowered anthropogenic optical depth, much of which is here due to absorption, is also reflected in the weakest ground surface forcing of the experiments ($-1.11\,Wm^{-2}$). Despite the strong reduction in the pre-industrial CDNC concentration, we also get the lowest estimate of the first indirect radiative forcing ($-1.65\,Wm^{-2}$). This seems to contradict the conclusion of Section 3.5, and in general results of tests showing that low background CDNC s lead to large indirect radiative forcing. The explanation is that the reduction in carbonaceous aerosol burden is predominant in the biomass burning areas, where the anthropogenic contribution to CDNC is reduced relatively more than the background CDNC. This is itself large enough to keep the cloud susceptibility low in these areas.

5. Discussion

5.1. The forcing of the first indirect effect

In the standard model version we use prescribed supersaturations to estimate CCN production, and we assume CDNC to equal the concentration of CCNs. However, we have recently introduced a more realistic treatment of cloud droplets which is similar to the method used in the earlier CAM2 based version of CAM-Oslo with a simpler aerosol module (Storelvmo et al., 2006). This method applies a prognostic equation for CDNC with source terms based on Abdul-Razzak and Ghan (2000), and calculates super-saturations based on a parameterized subgrid distribution of vertical velocities. Storelvmo et al. (2006) obtained a considerably smaller aerosol indirect forcing with this treatment. So far we have run this module for warm clouds in the most recent CAM-Oslo as a sensitivity test.

The improved CDNC treatment yields a considerable reduction of the first indirect forcing from $-1.78\,Wm^{-2}$ to $-1.13\,Wm^{-2}$, see Table 8 and Fig. 19. There are several aspects influencing this response. First of all, the more realistic scheme allows more possibilities for compensating effects. For example, when the super-saturation is calculated, its realized value depends on the availability of hygroscopic particles, their

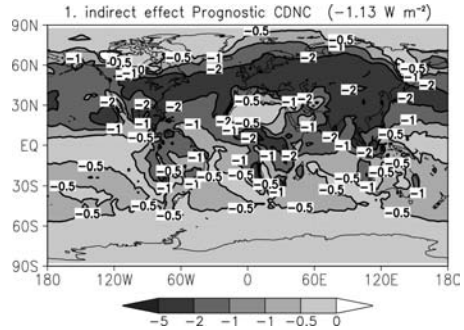

Fig. 19. As Figure 17, except that a prognostic equation for cloud droplet number concentrations is used. Unit: Wm^{-2}.

size, and the increase rate of the relative humidity. Hence, in the pre-industrial situation with considerably less SO_4 and OM than in the present-day situation, the realized super-saturation can be larger so that smaller particles are activated as CCNs. In the present-day situation, there can in addition be competition effects (Ghan et al., 1998) between SO_4, OM and in some cases SS, and even water soluble mineral dust. This may further reduce the maximum super-saturation compared to the pre-industrial situation, so that even fewer CCNs are activated. Furthermore, processes after CCN activation such as coalescence and washout by precipitation may reduce the effects of increased CCNs. From Table 8 we see that the mentioned effects for pre-industrial conditions in particular shows up at model level $\eta = 0.99$, and for present-day conditions at η-level 0.87. The anthropogenic increment in CDNC at this level decreases from 69 cm^{-3} in the standard simulation to 41 cm^{-3} in the case with prognostic CDNC. For η-level 0.99, which is close to the ground surface, the more advanced scheme leads to an increased anthropogenic increment in CDNC. The signal from warm clouds above the lowermost model layers will, however, dominate the effect on incoming solar radiation. Hence the indirect forcing is reduced with the more advanced scheme, in accordance with Penner et al. (2006).

5.2. *The direct radiative forcing*

With CAM-Oslo we have estimated a global anthropogenic DRF averaged over 3 yr to + 0.024 Wm^{-2}. This estimate is based on a 2-yr spin-up of the aerosol climatology from emissions. In comparison, the average DRF from the AeroCom (Schulz et al., 2006) is −0.22 Wm^{-2}, ranging from +0.04 to −0.41 Wm^{-2}. We have also compared with the recent estimate of −0.27 Wm^{-2} for ECHAM5-HAM (Stier et al., 2007). That value was estimated after only 3 months of spin-up. Our DRF estimated with similar spin-up would be −0.025 Wm^{-2}, that is as much as 0.05 Wm^{-2} smaller than the DRF given in Table 4. Compared to Stier et al. (2005, 2007) we employ a higher value for the imaginary part of the refractive index of BC. Based on recommendations by Bond and Bergstrom (2007) and better comparisons with absorption optical depth, Stier et al. (2007) recommend using a higher value than in Stier et al. (2005). After updating the BC refractive index, their estimated TOA DRF increases to −0.13 Wm^{-2}, with positive values over large areas.

Table 4. Total and absorptive AOD and direct radiative forcing by aerosols for simulation years 3–5

	Total – Pre-ind	Pre-ind – (SS+DU)	SS+DU
Aeosol optical depth (AOD)	0.0342	0.0174	0.0901
Absorption AOD	0.0025	0.0007	0.00081
TOA forcing (W m^{-2})	0.024	−0.198	−1.364
Surface forcing (W m^{-2})	−1.182	−0.592	−1.740

Table 5. Overview of 1-yr sensitivity tests. Each test starts from the same initial conditions. The tests are divided into two types for which C denotes cloud and precipitation processes, and S the assumed size and phase of primary aerosols

Standard	Modelled processes as described in main text
C1	Constituents directly below, under or inside clouds are affected by convective scavenging
C2	No mixing between convective updrafts and downdrafts
C3	Freeze-dry cloud parameterization is excluded
C4	Employs CAM3 auto-conversion to precipitation in warm clouds
S1	Assumes AeroCom emissions of accumulation and coarse mode SS.
S2	0.1% of coarse mode SS is assumed emitted in the Aitken mode
S3	Primary SO_4 emission is sulphuric acid gas in stead of accumulation mode particles
S4	Initial size of OM(a)/BC(a) is increased from 40 nm to 75 nm

Table 6. Calculated burdens and turnover times (τ) of the aerosol chemical components for each of the sensitivity experiments defined in Table 4. For the numbers in two rows, the upper values are for present day emissions and the lower are for pre-industrial. The emitted amounts of sea-salt and mineral dust are identical in the present day and pre-industrial simulations. Note that for the standard run (Std) and for the tests, results are for simulation year 5

Sens. test	SO_4 (Tg)	$\tau(SO_4)$ (d)	BC (Tg)	τ(BC) (d)	OM (Tg)	τ(OM) (d)	SS (Tg)	τ(SS) (d)	DU (Tg)	τ(DU) (d)
Std	2.00	4.01	0.14	6.79	1.31	7.30	5.79	0.27	10.4	2.26
	0.74	3.86	0.027	7.13	0.65	7.15				
C1	2.78	5.41	0.17	7.91	1.64	9.11	5.54	0.26	11.2	2.45
	1.02	5.09	0.034	8.91	0.81	8.93				
C2	2.50	4.97	0.18	8.72	1.72	9.55	6.61	0.31	11.1	2.43
	0.88	4.58	0.034	8.91	0.86	9.51				
C3	2.00	4.03	0.14	6.78	1.30	7.24	5.77	0.27	10.6	2.31
	0.74	3.85	0.027	7.07	0.64	7.08				
C4	1.89	3.86	0.14	6.71	1.29	7.21	5.48	0.26	10.2	2.23
	0.70	3.68	0.027	7.02	0.64	7.04				
S1	2.00	4.01	0.14	6.79	1.31	7.31	5.23	0.25	10.4	2.26
	0.74	3.86	0.027	7.13	0.65	7.16				
S2	1.99	4.00	0.14	6.76	1.31	7.26	5.81	0.27	10.4	2.26
	0.74	3.85	0.027	7.08	0.65	7.12				
S3	2.02	4.05	0.14	6.79	1.31	7.30	5.79	0.27	10.4	2.26
	0.75	3.90	0.027	7.13	0.65	7.15				
S4	2.00	4.01	0.11	5.05	0.80	4.45	5.79	0.27	10.4	2.26
	0.74	3.86	0.017	4.33	0.38	4.15				

Table 7. Calculated aerosol optical depth at 550 nm, direct radiative forcing, first indirect forcing, cloud droplet effective radii, and cloud droplet number concentrations (CDNC). The quantities $\eta = 0.87$ and 0.99 are model levels. Values are results for each of the sensitivity tests defined in Table 4. Numbers in two rows are values for present-day (upper) and pre-industrial (lower) emissions. Note that for the standard run (Std) and for the tests, results are for simulation year 5

	All sky optical depth	Aerosol direct TOA forcing (W m^{-2})	Aerosol direct Ground forcing (W m^{-2})	CDNC in $\eta = 0.87$ (cm^{-3})	Droplet Effective radius in $\eta = 0.87$ (μm)	CDNC in $\eta = 0.99$ (cm^{-3})	First aerosol Indirect forcing (W m^{-2})
Std	0.1413	0.031	−1.19	121.0	8.69	174.0	−1.78
	0.1071			52.0	9.43	99.0	
C1	0.1782	−0.057	−1.55	164.1	8.56	382.6	−1.88
	0.1320			71.5	9.31	211.4	
C2	0.1622	0.090	−1.52	118.3	8.61	157.2	−1.84
	0.1199			51.4	9.37	90.9	
C3	0.1405	0.040	−1.18	123.3	8.71	173.7	−1.80
	0.1067			52.9	9.47	98.4	
C4	0.1305	0.037	−1.18	118.0	8.56	166.8	−1.96
	0.0988			50.1	9.32	94.2	
S1	0.1101	0.014	−1.21	118.5	9.14	149.7	−1.95
	0.0751			48.1	10.01	73.6	
S2	0.1429	0.023	−1.12	126.5	8.53	194.7	−1.71
	0.1085			56.5	9.22	118.6	
S3	0.1398	0.045	−1.18	123.9	8.72	185.1	−1.74
	0.1067			54.4	9.43	100.6	
S4	0.1366	−0.071	−1.11	79.9	9.02	122.2	−1.65
	0.1048			36.4	9.69	72.9	

Table 8. Calculated cloud droplet number concentration and first aerosol indirect forcing at TOA for the standard simulation and for a simulation which solves a prognostic equation for cloud droplet number concentration according to Storelvmo et al. (2006). Numbers in two rows are for present-day (upper) and pre-industrial (lower) emissions. Results are for simulation years 3–5

	CDNC ($\eta = 0.87$) (cm^{-3})	CDNC ($\eta = 0.99$) (cm^{-3})	First aerosol, Indirect TOA forcing ($W\ m^{-2}$)
Standard	121.3	173.3	−1.78
	52.1	98.7	
Prognostic equation for CDNC	94.5	297.8	−1.13
	54.0	170.7	

Table 9. Estimated total and absorptive optical depth at 550 nm and direct radiative forcing for different assumptions for the mixing state of sulphate, BC and OM. Results for simulation year 5. When only one or two of the components are mentioned in the left column, the other(s) is(are) not included in the calculation of optical properties and radiation

	Anthropogenic optical depth	Anthropogenic absorptive optical depth	Aerosol direct TOA forcing ($W\ m^{-2}$)	Aerosol direct Ground forcing ($W\ m^{-2}$)
Standard	0.0342	0.00249	0.031	−1.19
Contribution by BC and OM	0.00730	0.00237	0.379	−0.792
Contribution by SO_4 only	0.0214	0.000014	−0.338	−0.326
Contribution by SO_4 and OM	0.0333	0.00018	-0.504	−0.604
Contribution by SO_4 and BC	0.0217	0.00180	0.164	−0.872
Non-absorptive OM	0.0342	0.00235	−0.018	−1.142
BC is externally mixed	0.0354	0.00174	−0.175	−1.024
No primary BC(ac) emitted	0.0338	0.00226	−0.021	−1.130

In the sensitivity tests the results are based on the year 5 with a 3-months spin-up after introducing test adjustments in the modelled aerosol. Hence there is little spin-up in aerosol concentration fields. The standard TOA radiative forcing for year 5 is $+0.031\ Wm^{-2}$. As mentioned in the introduction, there are many factors which combine to the direct aerosol radiative forcing. These factors need to be addressed if we want to understand the slightly positive direct forcing obtained with the standard simulation in this paper. We have already discussed some of the factors in the sensitivity tests in section 4, where it was shown that tests influencing the vertical aerosol mixing (C1 and C2) and size of carbonaceous aerosols (S4) gave large impacts on the DRF. C1 reduced and C2 increased the relative contribution of BC at middle and upper tropospheric levels. In cases where vertical transport and mixing of aerosols lead to layers of absorbing aerosols above clouds, the aerosols may decrease the planetary albedo. S4 increased the contribution of BC to particles in a size range which interacts efficiently with solar radiation, but at the same time the internally mixed OM and BC in this size range was efficiently activated as CCNs and scavenged by rain-out. In effect, the TOA radiative forcing was reduced by $0.1\ Wm^{-2}$ to $-0.071\ Wm^{-2}$.

Table 9 shows estimates of contributions of single or pairs of aerosol components to the global aerosol optical depth, aerosol absorptive optical depth, and to the anthropogenic radiative forcing. We only discuss contributions from SO_4, BC, and OM, which are the anthropogenic components in the model. Since the model calculates a variable degree of internal and external mixing and particle sizes depend on the amount of internally mixed mass, non-linear effects are possible. Chemical components which are not absorbing, such as SO_4, may thus contribute to aerosol absorption because mixing with BC increases the absorption as the BC-containing particles increase in size. This non-linear effect can be checked by adding the contribution to forcing from SO_4 alone (obtained by omitting both BC and OM from the optics and DRF calculations) to the combined contribution from BC and OM (obtained by omitting SO_4 from the optics and DRF calculations). The result is $0.041\ Wm^{-2}$, which is $0.010\ Wm^{-2}$ larger than the calculated standard result. This nonlinearity is largest in the lower troposphere at mid latitudes in the Northern Hemisphere. Otherwise, the contributions from each of the single components estimated as the difference between the standard forcing and the forcing due to the two remaining components are: $-0.369\ Wm^{-2}$ for SO_4, $+0.535\ Wm^{-2}$ for

BC and $-0.133\,\mathrm{Wm}^{-2}$ for OM. The corresponding multi-model average from AeroCom (Schulz et al., 2006) is respectively: $-0.35\,\mathrm{Wm}^{-2}$ for SO_4, $+0.25\,\mathrm{Wm}^{-2}$ for BC and $-0.14\,\mathrm{Wm}^{-2}$ for OM. Hence, in CAM-Oslo SO_4 and OM influence the TOA radiation balance as the average model, whilst BC contributes to the TOA forcing with about double strength compared to the average model.

Table 9 also shows results of a test where the imaginary refractive index of OM is set to a very low value (10^{-8}i). Thus, neglecting the slight absorption by OM which is assumed in the standard simulation (Köpke et al., 1997), the TOA DRF is reduced by $0.05\,\mathrm{Wm}^{-2}$ to $-0.018\,\mathrm{Wm}^{-2}$.

By condensation of sulphuric acid gas or by coagulation, BC is rapidly transferred into internally mixed particles. This process increases the particle size from nucleation or aitken modes to sizes which more efficiently interact with solar radiation. As shown by, for example Jacobson (2001) and Liao and Seinfeld (2005), an internal mixture of BC with other aerosol species gives a higher positive DRF than an external mixture. Table 9 also shows results from a test where BC is assumed externally mixed when calculating its optical properties, but without any influence on the calculated BC mass concentrations. The BC is then assumed hydrophobic with a standard aitken-mode size distribution. The anthropogenic TOA forcing is then decreased by more than $0.2\,\mathrm{Wm}^{-2}$ to $-0.175\,\mathrm{Wm}^{-2}$. This result emphasizes the importance of aerosol mixing.

We have assumed the existence of BC particle agglomerates which are emitted in the accumulation mode (Ström et al., 1992; Bond et al., 2006). These are considerably more slowly transformed into an internal mixture than BC emitted as nucleation mode particles. These BC particles are large enough to efficiently absorb solar radiation without internal mixing, even though their density is reduced due to the fluffy structures. In CAM-Oslo 36% of the average BC mass column is found above ca. 500 hPa, which is a larger fraction than most of the models in the AeroCom exercise. Most AeroCom models estimate between 10 and 25%, and one third above 30% (Textor et al., 2007). The highest fractions in CAM-Oslo are calculated in remote areas and in particular at high latitudes, where they exceed 60%. In our model 18% of the BC mass-column above 500 hPa is in the form of externally mixed BC agglomerates, and the fraction of the total BC column is 40% or larger in the high Arctic. Taking into account that only 10% of the fossil fuel BC emissions, or 4.2% of the total, is in this form, there is a factor of 5–10 enrichment in the relative contribution in remote areas. The final test in Table 9 investigates the effect of omitting the BC agglomerates denoted by BC(ac) in the table and in Figure 1. Also in this case, the TOA DRF is reduced with ca. $0.05\,\mathrm{Wm}^{-2}$ to $-0.021\,\mathrm{Wm}^{-2}$.

In Figure 20 we have compared the aerosol absorption optical depth in the model with retrieved data for a selection of AERONET sites. The sites are the same as those used for the comparison with the ECHAM5-HAM model (Stier et al., 2005), and the figure also compares with the data from that model.

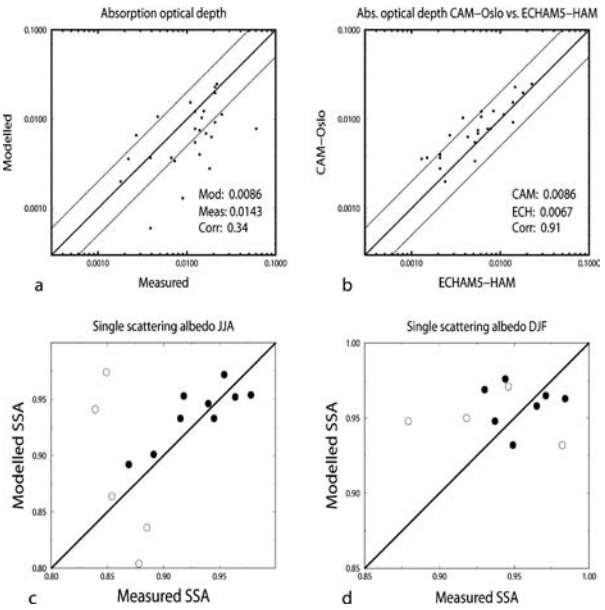

Fig. 20. Upper panel: Calculated versus observed aerosol absorption optical depth at 550 nm for (a) a selection of AERONET sites, and (b) compared with values from the model ECHAM5-HAM. Both measured and ECHAM5-HAM values are taken from Stier et al. (2005). Lower panel: Calculated versus observed values for the vertically integrated single scattering albedo at 550nm. The open circles are sites believed to be strongly influenced by emissions from biomass burning. The single scattering albedo is estimated as [1 – ABS/AOD], where ABS is the absorption optical depth. The AOD are taken from the same dataset as presented in Figure 12.

Hence, we see that the total aerosol absorption optical depth is about 40% under-estimated in our model. Notice also the very close agreement between the two model estimates on these sites, with our model producing about 20% higher values on average. We have also estimated and compared values of the column single scattering albedo for the same sites, and the agreement is good for sites close to fossil fuel BC emissions but much worse for sites that should be dominated by biomass burning BC emissions.

In conclusion, Figs. 20 and 6b leave no reason to assume that our model calculates an aerosol which absorbs too much solar radiation. Nevertheless, the absorption by BC is considerably more efficient for CAM-Oslo than for the average AeroCom model (Schulz et al., 2006). One possible source of this apparent anomalous behaviour of CAM-Oslo is that the aerosol mixing state is prescribed as external in several AeroCom models. A similar assumption in CAM-Oslo yields a $0.2\,\mathrm{Wm}^{-2}$ reduction in TOA radiative forcing. Other assumptions in CAM-Oslo, which possibly contribute to more aerosol absorption than many other models, include: emission of BC agglomerates from fossil fuel combustions; a small absorption by OM; emission of internally mixed OM and BC as aitken mode and not accumulation mode particles. Changing all these other assumptions could

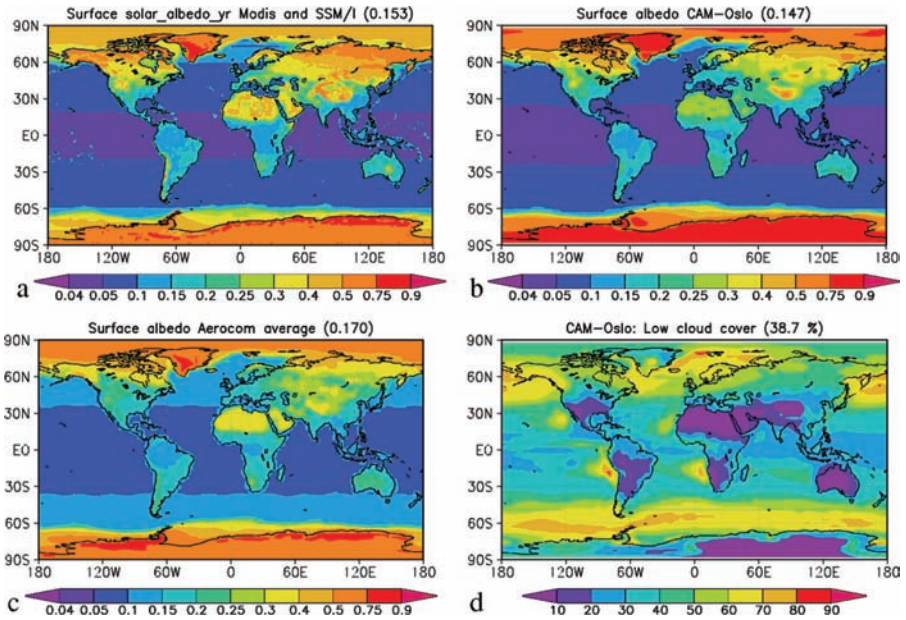

Fig. 21. (a) Surface albedo from Modis over land and calculated according to solar angle over sea; (b) Calculated surface albedo from CAM-Oslo; (c) Calculated surface albedo averaged for the AeroCom models and (d) Low-level cloud cover in CAM-Oslo. Data for a) and c) are obtained from S. Kinne (pers. comm.). The shown albedo data are for broadband solar radiation (0.2–5.0 μm).

easily reduce the TOA radiative forcing by more than 0.2 Wm^{-2}. However, we have no good reason for doing such changes, even though the results would be less surprising.

Other factors than aerosol optical properties influence the TOA DRF, in particular the ground surface albedo and the low tropospheric cloudiness are important. Figure 21 shows the annual mean ground surface, broad band albedo in CAM-Oslo (global: 0.147), the AeroCom average (global: 0.170), and a synthesis of model data over oceans, MODIS retrievals over continents, and SSM/I retrievals for snow and ice (global: 0.153), obtained from S. Kinne (personal communication). Our ground surface albedo is generally smaller than both the satellite retrievals and the AeroCom average. One important exception is found for high latitudes, where CAM-Oslo has larger albedo values. This high albedo in the Arctic and the enriched BC agglomerates modelled at high latitudes contribute in combination to absorption of solar radiation globally.

The last map in Fig. 21 shows that low level clouds are ubiquitous in many regions, and in particular over mid- and high-latitude oceans and adjacent, down-wind continents. The globally averaged low cloud cover is almost 40%, which is considerable. For comparison, the low cloud fraction from the International Satellite Cloud Climatology project, ISCCP (Rossow and Dueñas, 2004), is only 28%, although these data are uncertain.

6. Summary and conclusions

The former aerosol-climate modelling system CCM-Oslo has been updated to CAM-Oslo. CAM-Oslo is based on the NCAR atmospheric general circulation model CAM3. We have extended this model with an aerosol life-cycle module which enables *a posteriori* estimates of size distributions, optical properties and contributions to CCN. Effects of aerosols on radiation and clouds are thus calculated on-line through look-up tables. The background of primary particles includes both explicitly calculated modes of SS and mineral dust, emitted aitken and accumulation mode primary particles, and nucleated new sulphate particles. The latter is produced if there is a surplus of sulphuric acid gas left after condensation on pre-existing particles.

Calculated burdens and lifetimes are within the range found in the AeroCom model intercomparison (Textor et al., 2006), although on the low side in the case of mineral dust and in particular SS. Despite the short lifetime of SS, the model compares well with measurements with a tendency to overestimate at continental measurement sites. On the other hand the model considerably underestimates the concentrations of mineral dust away from the major emission sources (factor $\sim$2), to some extent caused by the assumed hygroscopic coating but primarily by missing non-desert dust emissions. Sulphate and carbonaceous aerosols compare well with measurements, but with slight under-estimates for BC and OM. The measurements of BC and OM are fewer and more uncertain and the data are mainly confined to North America.

Modelled versus retrieved optical depths confirm that the column burdens of aerosol particles are too low. The simulated clear sky AOD of 0.12 is lower than both AERONET (0.14) and MODIS-MISR (0.16). These underestimates are especially pronounced over regions dominated by biomass burning emissions and in non-Saharan semi-arid regions, as well as over the western

and northern part of the Indian Ocean. Over the Indian Ocean the model has too much precipitation and hence too high scavenging. Other possible explanations of the underestimates are inaccuracies in the parameterization of convective scavenging, and uncertain emissions. For Europe and North America the yearly average is quite good, but the model has almost no seasonal cycle in AOD. The measurements and retrievals on the other hand have a distinct summer maximum. We emphasize, however, that if the model had been perfect with regard to the aerosols included in the model, the AOD should be underestimated since emissions of some aerosol components are not included, such as nitrate, biogenic material and non-desert mineral dust.

Globally the model calculated Ångström parameter compares well with Aeronet data and in particular over land areas at low and mid-latitudes. At higher latitudes the sample spread is larger, and too small values occur more frequently than too large values. Due to a combination of efficient vertical convective transport, the internal mixing between light absorbing BC and water-soluble components, the emitted fossil fuel BC agglomerates in the accumulation mode, the high ground surface albedo at high latitudes, and possibly also too much low level clouds, we get a slightly positive direct global radiative forcing at the TOA of $0.026\,\mathrm{Wm}^{-2}$. The high absorption also contributes to a negative surface radiative forcing of $-1.13\,\mathrm{Wm}^{-2}$. The slightly positive DRF at TOA is not very sensitive to changes in total anthropogenic column burdens, but changes somewhat with varying amount of carbonaceous particles in the upper troposphere. Despite the condensational growth on aitken mode particles, we calculate a low CDNC, especially in remote pristine areas with values as low as $10\,\mathrm{cm}^{-3}$ over the southern subpolar oceans. The low modelled pre-industrial CDNC contributes to a high estimate of the first indirect (albedo) effect: $-1.78\,\mathrm{Wm}^{-2}$. Compared to the aerosol direct effect, the modelled indirect effect depends more on the aerosol number concentrations and meteorological parameters during pre-industrial conditions, like the cloud LWP. This finding is in line with other sensitivity studies where a large change in indirect forcing is found for even small changes in the background level of CDNC (Lohmann et al., 2000; Storelvmo et al., 2006; Kirkevåg et al., 2008b). Finally, by introducing prognostic equations for CDNC coupled to calculated super-saturations based on a subgrid distribution of vertical velocities, compensating effects reduce the first indirect forcing by ca. 36% to $-1.13\,\mathrm{Wm}^{-2}$.

In this paper, we have not tuned any aerosol related variables in order to reduce the model biases relative to observations or retrievals. In consequence, the results are expected to yield systematic errors that are attributable to concentration levels. In particular, we considerably underestimate mineral dust concentrations. Non-desert emissions are neglected. We also underestimate carbonaceous aerosol concentrations; and secondary anthropogenic contributions are so far neglected. Neglected are also particulate nitrate and biological particles. Underestimating the number of background aerosol particles may increase the relative importance of anthropogenic aerosols on the indirect forcing.

7. Acknowledgments

This research has been supported by the Norwegian Research Council through the AerOzClim, RegClim, and NorClim projects. The work has also received support from the Norwegian Research Council's program for Supercomputing through a grant of computing time. We gratefully acknowledge the cooperation and discussions with J. E. Kristjánsson and A. Grini. This work has benefited greatly from being allowed to use observational data from the AEROCE, AERONET, AIRMON, EMEP, GAW and IMPROVE networks, and thanks are due to S. Guibert, M. Schulz and S. Kinne for preparing the data. Sulphate data in Figure 5 are obtained through J. Prospero and D. Savoie. S. Kinne has most kindly provided satellite data on aerosol optical depth and ground surface albedo. We are grateful to R. Easter for providing the dry deposition and part of the chemistry code. We gratefully acknowledge P. J. Rasch and S. Ghan for sharing code and scientific advice under the development of CAM-OSLO. Two anonymous reviewers helped improve the first version of the manuscript.

References

Albrecht, B. A. 1989. Aerosols, cloud microphysics and fractional cloudiness. *Science* **245**, 1227–1230.

Abdul-Razzak, H. and Ghan, S. J., 2000. A Parameterization of aerosol activation. Part 2: multiple aerosol types. *J. Geophys. Res.* **105**(D), 6837–6844.

Baker, M. B., 1993. Variability in concentrations of cloud condensation nuclei in the marine cloud-topped boundary layer. *Tellus* **45B**, 458–472.

Barth, M. C., Rasch, P. J., Kiehl, J. T., Benkowitz, C. M. and Schwartz, S. E. 2000. Sulphur chemistry in the National Center for Atmospheric Research Community Climate Model: Description, evaluation, features, and sensitivity to aqueous chemistry. *J. Geophys. Res.* **105**, 1387–1415.

Berntsen, T. K. and Isaksen, I. S. A., 1997. A global three-dimensional chemical transport mode for the troposphere. 1. Model description and CO and ozone results. *J. Geophys. Res.* **102**, 21239–21281.

Binkowski, F. S. and Shankar, U., 1995. The Regional Particulate Matter Model: 1. Model description and preliminary results. *J. Geophys. Res.* **100**, 26191–26209.

Bond, T. C. and Bergstrom, R. W. 2006. Light Absorption by carbonaceous particles: An investigative review. *Aerosol Sci Technol.* **40**, 27–68.

Bond, T. C., Wehner, B., Plewka, A., Wiedensohler, A., Heintzenberg, J. and Charlson, R. J., 2006. Climate-relevant properties of primary particulate emissions from oil and natural gas combustion. *Atmos. Environ.* **40,** 3574–3587.

Boville, B. A., Rasch, P. J., Hack and McCaa, J. R. 2006. Representation of Clouds and Precipitation Processes in the Community Atmosphere Model Version 3. *J. Climate* **19**, 2184–2198.

Charlson, R. J., Schwartz, S. E., Hales, J. M., Cess, R. D., Coakley, and co-authors. 1992. Climate forcing by anthropogenic aerosols. *Science* **255**, 423–430.

Chen, C. and Cotton, W. R. 1987. The physics of the marine stratocumulus-capped mixed layer. *J. Atmos. Sci.* **44**, 2951–2977.

Chuang, C. C. and Penner, J. E. 1995. Effects of anthropogenic sulphate on cloud drop nucleation and optical properties. *Tellus* **47B**, 566–577.

Collins, W. D., Rasch, P. J., Boville, B. A., Hack, J. J., McCaa, J. R. and co-authors. 2004. *Description of the NCAR Community Atmosphere Model (CAM3)*. Tech. Rep. NCAR/TN-464+STR, National Center for Atmospheric Research, Boulder, CO, 226 pp.

Collins, W. D., Rasch, P. J., Boville, B. A., Hack, J. J., McCaa, J. R. and co-authors. 2006a. The Formulation and atmospheric simulation of the Community Atmospheric Model Version 3 (CAM3). *J. Climate* **19**, 2144–2161.

Collins, W. D., Bitz, C. M., Blackmon, M. L., Bonan, G. B., Bretherton, and co-authors. 2006b. The Community Climate System Model Version 3 (CCSM3). *J. Climate* **19**, 2122–2143.

Cooke, W. F. and Wilson, J. J. N., 1996. A global black carbon aerosol model. *J. Geophys. Res.* **101**, 19305–19409.

Dentener, F., Kinne, S., Bond, T., Boucher, O., Cofala, J. and co-authors. 2006. Emissions of primary aerosols and precursor gases in the years 2000 and 1750 prescribed data-sets for AeroCom *Atm. Chem. Physics* **6**, 4321–4344.

Dubovik, O., Holben, B., Eck, T. F., Smirnov, A., Kaufman, Y. J. and co-authors. 2002. Variability of absorption and optical properties of key aerosol types observed in worldwide locations. *J. Atm. Sci.* **59**, 590–608.

Dusek, U., Frank, G. P., Hildebrandt, L., Curtius, J., Schneider, J. and co-authors. 2006. Size matters more than chemistry for cloud-nucleating ability of aerosol particles. *Science* **312**, 1375–1378.

Easter, R. C., Ghan, S. J., Zhang, Y., Saylor, R. D., Chapman, E. G. and co-authors. 2004. Mirage: Model description and evaluation of aerosols and trace gases. *J. Geophys. Res.* **109**, D20210, doi:10.1029/2004JD004571.

Ghan, S. J., Leung, L. R., Easter, R. C. and Abdul Razzak, H. 1997. Prediction of droplet number in a general circulation model. *J.Geophys.Res.* **102**, 21777–2194.

Ghan, S. J., Guzman, G. and Abdul-Razzak, H. 1998. Competition between sea salt and sulfate particles as cloud condensation nuclei. *J. Atmos. Sci.* **55**, 3340–3347.

Ghan, S. J., Laulainen, N., Easter, R., Wagener, R., Nemesure, S. and co-authors. 2001. Evaluation of aerosol direct radiative forcing in MIRAGE. *J. Geophys. Res.* **106**(D6), 5295–5316.

Guyon, P. Boucher, O., Graham, B., Beck, J.,Mayol-Bracero, O. L. and co-authors. 2003. Refractive index of aerosol particles over the Amazon tropical forest during LBA-EUSTACH 1999. *J. Aerosol Sci.* **34**(7), 883–907.

Hack, J. .J., Caron, J. M., Yeager, S. G., Oleson, K. W., Holland, M. M. and co-authors. 2006. Simulations of the global hydrological cycle in the CCSM Community Atmosphere Model Version 3 (CAM3): Mean features. *J. Climate* **19**, 2199–2221.

Han, Q., Rossow, W. B. and Lacis, A. A., 1994. Near-global- survey of effective droplet radii in liquid water clouds using ISCCP data. *J. Clim.* **7**, 465–497.

Harrison, E. F., Minnis, P., Barkstrom, B. R., Ramanathan, V., Cess, R. D. and co-authors. 1990. Seasonal variation of cloud radiative forcing derived from the Earth Radiation Budget Experiment. *J. Geophys. Res.* **95,** 18687–18703.

Henze, D. K. and Seinfeld, J. H., 2006. Global secondary organic aerosol from isoprene oxidation. *Geophys. Res. Lett.* **33**, L09812, doi:10.1029/2006GL025976.

Iversen, T. and Seland, Ø. 2002. A scheme for process-tagged SO_4 and BC aerosols in NCAR-CCM3. Validation and sensitivity to cloud processes. *J. Geophys. Res.* **107**(D24), 4751, doi:10.1029/2001JD000885.

Iversen, T. and Seland, Ø. 2003. Correction to "A scheme for process-tagged SO_4 and BC aerosols in NCAR-CCM3. Validation and sensitivity to cloud processes". *J. Geophys. Res.* **108**(D16), 4502, doi:10.1029/2003JD003840.

Iversen, T. and Seland, Ø. 2004. The role of cumulus parameterisation in global and regional sulphur transport. In: *Air Pollution Modeling and Its Application XVI*, (Eds Borrego, C. and Incecik, S.), 225–233. Kluwer Academic Publications, New York.

Iversen, T., Kirkevåg, A., Kristjánsson, J. E. and Seland, Ø. 2001. Climate effects of sulfate and black carbon estimated in a global climate model. In: *Air Pollution Modeling and Its Application XIV*, (Eds Gryning, S.-E. and Schiermeier, F. A.) 335–342, Kluwer Acad., Norwell, Mass.

Iversen, T., Kristjánsson, J. E., Kirkevåg, A. and Seland, Ø. 2005. Calculated feedback effects of climate change caused by anthropogenic aerosols. RegClim General Technical Report **No. 8**, 111–120.

Jacobson, M., 2001. Strong radiative heating due to the mixing state of black carbon in atmospheric aerosols. *Nature* **409**, 695–697.

Jaenicke, R. 2005. Abundance of cellular material and proteins in the atmosphere. *Science* **308**, 73.

Janzen, J. 1979. The refractive index of colloidal carbon. *J. Colloid and Interface Sci.* **69**(3), 436–447.

Kiehl, J. T. and Trenberth, K. E. 1997. Earth's Annual Global Mean Energy Budget. *Bull. Am. Meteorol. Soc.* **78,** 197–208.

Kiehl, J. T., Hack, J. J., Bonan, G. B., Boville, B. B.., Williamson, D. L. and co-authors. 1998. The National Center for Atmospheic Research Community Climate Model: (CCM3). *J. Climate* **11**, 1131–1149.

Kiehl, J. T., Schneider, T. L., Rasch, P. J. and Barth, M. C. 2000. Radiative forcing due to sulfate aerosols from simulations with the National Center for Atmospheic Research Community Climate Model, Version 3. *J. Geophys. Res.* **105**(D1), 1441–1457.

Kinne, S., Schulz, M., Textor, C., Guibert, S., Balkanski, Y. and co-authors. 2006. An AeroCom initial assessment - optical properties in aerosol component modules of global models. *Atm. Chem. Phys.* **6**, 1815–1834.

Kirkevåg, A. and Iversen, T. 2002. Global direct radiative forcing by process-parameterized aerosol optical properties. *J. Geophys. Res.* **107**(D20), 4433, doi:10.1029/2001JD000886.

Kirkevåg, A., Iversen, T., Seland, Ø. and Kristjánsson, J. E. 2005. Revised schemes for aerosol optical parameters and cloud condensation nuclei in CCM-Oslo. *Institute Report Series*, Department of Geosciences, University of Oslo, 29 pp, ISBN 82-91885-31-1, ISSN 1501-6854-128.

Kirkevåg, A., Iversen, T., Kristjánsson, J. E., Seland, Ø. and Debernard, J. B. 2008a. On the additivity of climate response to anthropogenic aerosols and CO_2, and the enhancement of future global warming by carbonaceous aerosols. *Tellus 60 A this issue*.

Kirkevåg, A., Iversen, T., Seland, Ø., Debernard, J. B., Storelvmo, T. and co-authors. 2008b. Aerosol-cloud-climate interactions in the climate model CAM-Oslo. *Tellus 60 A this issue*.

Koch, D., Schmidt, G. A. and Field, C. V. 2006. Sulfur, sea salt and radionuclide aerosols in GISS ModelE. *J. Geophys. Res.* **111**, D06206, doi:10.1029/2004JD005550.

Köpke, P., Hess, M., Schult, I. and Shettle, E. P., 1997. *Global Aerosol Data Set*. MPI Report no. 243.

Kristjánsson, J. E. 2002. Studies of the aerosol indirect effect from sulfate and black carbon aerosols. *J. Geophys. Res.* **107**(D15), 4246, doi:10.1029/2001JD000887.

Kristjánsson, J. E., Iversen, T., Kirkevåg, A., Seland, Ø. and Debernard, J. 2005. Response of the climate system to aerosol direct and indirect forcing: Role of cloud feedbacks. *J. Geophys. Res.* **110**, D24206, doi:10.1029/2005JD006299.

Liao, H. and Seinfeld, J. 2005. Global impacts of gas-phase-chemistry-aerosol interactions on direct radiative forcing by anthropogenic aerosols and ozone. *J. Geophys. Res.* **110**(D18), D18208, 4297, doi:10.1029/2005JD005907.

Liu, L., Lacis, A. A. Carlson, B. E. Mishchenko, M. I. and Cairns, B. 2006. Assessing Goddard Institute for Space Studies ModelE aerosol climatology using satellite and ground-based measurements: A comparison study. *J. Geophys. Res.* **111**, D20212, doi:10.1029/2006JD007334.

Lohmann, U. and Feichter, J. 2005. Global indirect aerosol effects: a review. *Atmos. Chem. Phys.* **5**, 715–737.

Lohmann, U. and Leck, C. 2005. Importance of submicron surface-active organic aerosols for pristine Arctic clouds. *Tellus* **57B**, 261–268.

Lohmann, U., Feichter, J., Penner, J. E. and Leaitch, W. R. 2000. Indirect effect of sulfate and carbonaceous aerosols: A mechanistic treatment. *J. Geophys. Res.* **105**, 12193–12206.

Mårtensson, E. M., Nilson, E. D., de Leeuw, G., Cohen, L. H. and Hansson, H.-C., 2003. Laboratory simulations and parameterization of the primary marine aerosol production. *J. Geophys. Res.* **108**(D9), 4297, doi:10.1029/2002JD002263.

Ogren, J. A. and Charlson, R. J. 1983. Elemental carbon in the atmosphere: Cycle and lifetime. *Tellus* **35B**, 241–254.

Penner, J. E., Quaas, J., Storelvmo, T., Takemura, T., Boucher, O. and co-authors. 2006. Model intercomparison of indirect aerosol effects. *Atm. Chem. Phys.* **6**, 3391–340.

Quian, Y., Kaiser, D. P., Leung, L. R. and Xu, M. 2006. More frequent cloud-free sky and less surface solar radiation in China from 1955-2000. *Geoph. Res. Letters* **33**, L01812, doi:10.1029/2005GL024586.

Rasch, P. J. and Kristjánsson, J. E. 1998. A comparison of the CCM3 model climate using diagnosed and predicted condensate parameterizations. *J. Climate* **11**, 1587–1614.

Rogers, R .R. and Yau, M. K., 1989. *A short course in cloud-physics*, International series in Natural Philosophy volume 113, Pergamon Press.

Rossow, W. B. and Dueñas, E. N. 2004. The international Satellite Cloud Climatology Project (ISCCP). *Bull. Am. Meteorol.* **85**, 167–172.

Schulz, M., Textor, C., Kinne, S., Balkanski, Y., Bauer, S. and co-authors. 2006. Radiative forcing by aerosols as derived from the AeroCom present-day and pre-industrial simulations. *Atm. Chem. Phys.* **6**, 5225–5246.

Schmidt, G. A., Ruedy, R., Hansen, J. E., Aleinov, I., Bell, N. and co-authors. 2006. Present day atmospheric simulations using GISS ModelE: Comparison to in-situ, satellite and reanalysis data, *J. Climate* **19**, 153–192.

Seinfeld, J. H. and Pandis, S. N. 1998. *Atmospheric Chemistry and Physcis: From Air Pollution to Climate Change*, 1326 pp., John Wiley, New York.

Slingo, A., 1989. A GCM parameterisation for the shortwave radiative properties of water clouds. *J.Atmos.Sci.* **46**., 1419–1427.

Sokolik, I. N. and Toon, O. B. 1999. Incorporation of mineralogical composition into models of the radiative properties of mineral aerosol from UV to IR wavelengths. *J. Geophys. Res.* **104**(D8), 9423–9444.

Solomon, S., Qin, D., Manning, M., Alley, R. B., Berntsen, T. and co-authors. 2007. Technical Summary. In: *Climate Change 2007: The Physical Science Basis. Contribution of Working Group I to the Fourth Assessment Report of the Intergovernmental Panel on Climate Change* (Eds Solomon, S., Qin, D., Manning, M., Chen, Z., Marquis, M., Averyt, K. B., Tignor, M. and Miller, H. L.). Cambridge University Press, Cambridge, United Kingdom and New York, NY, USA.

Stier, P., Feichter, J., Kinne, S., Kloster, S., Vignati, E. and co-authors. 2005. The aerosol-climate model ECHAM5-HAM. *Atmos. Chem. Phys.* **5**, 1125–1156.

Stier, P., Seinfeld, J. H., Kinne, S. and Boucher, O. 2007. Aerosol absorption and radiative forcing. *Atmos. Chem. Phys.* **7**, 5237–5261.

Storelvmo, T., Kristjánsson, J. E., Ghan, S., Kirkevåg, A., Seland, Ø. and Iversen, T. 2006. Predicting cloud droplet number in CAM-Oslo. *J. Geophys. Res.* **111**, D24208, doi:10.1029/2005JD006300.

Ström, J. S., Okada, K. and Heintzenberg, J. 1992. On the state of mixing of particles due to Brownian coagulation. *J. Aerosol Sci.* **23**, 467–480.

Textor, C., Schulz, M., Guibert, S., Kinne, S., Balkanski, and co-authors. 2006. Analysis and quantification of the diversities of aerosol life cycles within AeroCom. *Atmos. Chem. Phys.* **6**, 1777–1813.

Textor, C., Schulz, M., Guibert, S., Kinne, S., Balkanski, Y. and co-authors. 2007. The effect of harmonized emissions on aerosol properties in global models – an AeroCom experiment. *Atmos. Chem. Phys. Discuss.* **7**, 1699–1723.

Twomey, S. 1977. The Influence of Pollution on the Shortwave Albedo of Clouds, *J. Atmos. Sci.* **34**, 1149–1152.

Vignati, E., Wilson, J. and Stier, P., 2004. M7: a size resolved aerosol mixture module for the use in global aerosol models. *J. Geophys. Res.* **109**, D22 202, doi:10.1029/2003JD004485.

Wesely, M. L., 1989. Parameterization of surface resistances to gaseous dry deposition in regional-scale numerical Models. *Atmos. Environ.* **23**, 1293–1304.

Wilson, J., Cuvelier, C. and Raes, F. 2001. A modelling study of global mixed aerosol fields. *J. Geophys. Res* **106**, 34081–34108.

Xu, K.-M. and Randall, D. A. 1996. A Semiempirical Cloudiness Parameterization for Use in Cloud Models. *J. Atmos.Sci.* **53**, 3084–3102.

Zhang, G. J. and McFarlane, N. A. 1995. Sensitivity of climate simulations to the parameterization of cumulus convection in the Canadian Climate Centre general circulation model. *Atmos. Ocean* **33**, 407–446.

Zhang, M., Lin, W., Bretherton, C. S., Hack, J. J. and Rasch, P. J. 2003. A modified formulation of fractional stratiform condensation rate in the NCAR Community Atmospheric Model (CAM2). *J. Geophys. Res* **108**, 4035, doi:10.1029/2002JD002523.

Zhang, Y., Easter, R., Ghan, S. J. and Abdul-Razzak, H. 2001. Impact of aerosol size representation on modeling aerosol-cloud interactions. *J. Geophys. Res* **107**, doi:10.1029/2001JD001549.